A 9-node co-rotational curved quadrilateral shell element for smooth, folded and multi-shell structures

Z. X. Li[1] T. Z. Li[1] L Vu-Quoc[2] B. A. Izzuddin[3] X. Zhuo[1] Q. Fang[3]

[1]Department of Civil Engineering, Zhejiang University, Hangzhou 310058, China

[2]Aerospace Engineering, University of Illinois at Urbana-Champaign, Urbana, IL 61801, USA

[3]Department of Civil and Environmental Engineering, Imperial College London, SW7 2BU, UK

Summary

A 9-node co-rotational curved quadrilateral shell element with novel treatment for rotation at intersection of folded and multi-shell structures is presented. The element's co-rotational reference frame is defined by the two bisectors of the diagonal vectors generated using the four corner nodes and their cross product. In reference frame, the element rigid-body rotations are excluded in calculating the local nodal variables from the global nodal variables. Rotations are not represented by axial (pseudo) vectors, but by components of polar (proper) vectors, of which additivity and commutativity lead to symmetry of the tangent stiffness matrix. In the global coordinate system, the two smallest components of the mid-surface normal vector at each node of a smooth shell, or at nodes away from the intersection of non-smooth shells, are defined as rotational variables. In addition, of the two nodal orientation vectors at intersections of folded and multi-shell structures, two smallest components of one vector, together with one smaller component of another vector, are employed as rotational variables, leading to the desired additive property for all nodal variables in a nonlinear incremental solution procedure. In the local coordinate system, the two smallest components of the mid-surface normal vector(s) at any node of a smooth shell, or in each smooth patch of non-smooth shell, are defined as rotational variables. Different from other existing co-rotational finite-element formulations, the resulting element tangent stiffness matrix is symmetric owing to the commutativity of the local nodal variables in calculating the second derivative of strain energy with respect to these nodal variables. To alleviate membrane and shear locking phenomena, the membrane strains and the out-of-plane shear strains are replaced with assumed strains, using the Mixed Interpolation of Tensorial Components (MITC) approach, for obtaining the element tangent stiffness matrices and the internal force vector. Finally, a series of benchmark, challenging smooth,

folded and multi-shell structures undergoing large displacements and large rotations are analyzed to demonstrate the reliability and computational accuracy of the proposed formulation.
Keywords: Curved quadrilateral shell element; Co-rotational approach; Vectorial rotational variable; Folded and multi-shell structures; Locking free; Assumed-strain method

1. Introduction

Folded and multi-shell structures are widely used in engineering practice, such as thin-walled steel beams and columns, pressure vessels, silos, liquid and gas storage tanks, tubular towers, branching and intersecting pipelines, etc. In most of such multi-shells, the adjacent elements are usually stiffly connected to each other. But there also exist simply connected and partly simply supported shell junctions as well as the elastically and dissipatively deformable shell junctions [1-5]. In this paper, only rigid junctions (the deformation of the multi-shell structure has no effect on the angle between the middle surfaces of the two shells at the junction) are considered, and the intersection of irregular shell structures are treated as curved lines between different smooth shell patches with their mid-surface interconnected non-smoothly.

Different rotation parameters can be employed in shell elements [6-14]. In most existing finite element formulations based on classical shell theory, even though the rotation around the normal to the shell mid-surface are disregarded, these elements still demonstrate satisfying performance in modeling of smooth shell structures. Classical shell theory did not, however, achieve the same level of success in finite element modeling of non-smooth shell structures (such as folded shells and multi-shells) and connections of shells with beams, columns and stiffeners. The absence of a rotation component around the shell director makes it difficult to impose continuity at the branching points, or provide a compatible connection with a beam model [15-17]. To circumvent such problems, some researchers attempt to impose appropriate kinematic constraints at the branching points [17], or work in a local coordinate system which is aligned with the shell boundary [17]. Unfortunately, the former is sensitive to numerical ill-conditioning in shallow shell geometry, while the latter is cumbersome in numerical implementation [17]. To facilitate the modeling of non-smooth shell structures, some researchers introduced the drilling rotation component in developing finite element formulations, leading to shell finite elements with three rotation parameters per node [17-26]. Ibrahimbegovic and Frey [17-19] proposed a consistent formulation of geometrically-linear shell

theory with drilling rotations by consistent linearization of geometrically non-linear shell theory. Chroscielewski et al.[20] proposed constitutive relations for composite shells within the framework of 6-parameter shell theory with drilling degree of freedom. Fox and Simo [21] obtained a three rotational degree of freedom formulation by enforcing weakly the kinematic constraint to identify the drilling rotation via a Lagrange multiplier term appended to the variational principle of the classical model. Since the corresponding Lagrange multiplier is shown to vanish at equilibrium, it is possible to construct a regularization of this constrained variational principle which yields the equilibrium equations for any value of the regularization parameter. Witkowski [22] presented a 4-node C_0 shell element with drilling degrees of freedom within the nonlinear 6-field shell theory, where kinematics of the shell is described by the vector field of translations and the orthogonal tensor field of rotations, and no restriction is applied on magnitudes of displacements and rotations. Ibrahimbegovic and Wilson [23] obtained a unified formulation for triangular and quadrilateral flat shell finite-elements with 6 nodal degrees of freedom by superposing discrete Kirchhoff plate bending elements and the membrane elements with drilling degrees of freedom. Kebari and Cassell [24] presented a nine-node degenerate stress-resultant shell element with 6 degrees of freedom at each node and the sixth dof is incorporated by using the penalty function method.

Some difficulties are encountered in numerically implementing shell finite elements with drilling rotations, since the stiffness due to three rotations arises merely from the intersection of surfaces, whereas the stiffness due to the drilling rotation at any node away from the intersection of non-smooth shell is very low or even zero, thus numerical problems arise if a drilling rotation is employed at every node. This problem can be prevented by a classification of nodes – either located in the smooth areas or on the intersections. There is no general criterion to automatically distinguish these two types of nodes, thus requiring a manual classification. Alternatively, some kind of drilling rotation stabilization can be used [27-28]. To handle geometries with junctions and allowing for arbitrary intersections of patches, Dornisch and Klinkel [28] presented an enhanced isogeometric Reissner-Mindlin shell formulation which neither requires drilling rotation stabilization, nor user interaction to quantify the number of rotational degrees of freedom for every node. They assigned control points with corresponding physical location to one common node for the finite element solution, and defined a nodal basis system in every control point, which ensures an exact interpolation of the director vector throughout the whole domain. To avoid the problem of drilling

degrees of freedom, several researchers developed solid-shell elements [29-33], in which nodal displacements are the only degrees of freedom, thus finite-rotation axial (pseudo) vectors and their complex update procedures are entirely avoided. Effective treatments for shear locking, membrane locking, trapezoidal locking, and Poisson thickness locking must, however, be introduced [29-33].

In the present 9-node co-rotational curved quadrilateral shell element formulation for smooth, folded and multi-shells, the Reissner-Mindlin theory is employed, allowing for shear deformation. Rotation is represented not by axial (pseudo) vector, but by components of polar (proper) vector, of which additivity and commutativity lead to symmetry of the tangent stiffness matrix. At any node of a smooth shell, or at a node away from the intersection of non-smooth shells, the two smallest components of the mid-surface normal vector in the global coordinate system are selected as vectorial rotational variables [34]. Such vectorial rotational variables had been successfully employed in developing 4-node and 9-node quadrilateral elements, 3-node and 6-node triangular elements accommodating elastic or elasto-plastic or composite behavior for smooth shells undergoing large displacement and large rotations [35-40]. On the other hand, at a node on the intersection edge of non-smooth shells, we introduce a novel treatment of rotation (without using an axial rotation vector) by using two smallest components of one vector and one smaller component of another vector of a triad oriented initially to three axes of the global coordinate system as vectorial rotational variables. These vectorial rotational variables could be different components of the same (polar / proper) vector(s) even at the same node in different incremental steps of a nonlinear incremental solution procedure. Two smallest components of the mid-surface normal vector are defined as vectorial rotational variables at any node of smooth or non-smooth shells in the local coordinate system. To alleviate the membrane and shear locking phenomena, the membrane strains and the out-of-plane shear strains are replaced with assumed strains in calculating the element strain energy. The tying point scheme used in the MITC approach [41] is employed in the calculation of the assumed strains. Different from the MITC isotropic quadrilateral shell finite element formulations using linear covariant natural strain tensor, in the present 9-node curved quadrilateral shell element formulation:

1) The linear covariant natural strain tensor is replaced with the Green-Lagrange strains specialized for shallow curved shell (with nonlinear terms);

2) A co-rotational framework is adopted in calculating the local internal force vector and

element tangent stiffness matrix.

In other existing co-rotational element formulations, most researchers employed axial vectors to represent rotations, and thus used non-vectorial rotational variables, enforcing the semi-tangential behaviour of nodal moments through a correction matrix to the conventional geometric stiffness matrix [42-48]. Felippa and Haugen [45] presented a co-rotational formulation, using spin (coming from the derivative of the rotation matrix) instead of rotation axial vector as nodal degree of freedom, that lead to non-symmetric geometric tangent stiffness matrix, and thus non-symmetric tangent stiffness matrix. Due to the non-commutativity of finite rotations about fixed axes, this method always leads to a non-symmetric tangent stiffness matrix [43-54]. Crisfield and his co-workers [43,46] also encountered this phenomenon, and artificially symmetrized the element tangent stiffness matrix by excluding the non-symmetric term. While this treatment can greatly improve the computational efficiency, quadratic convergence of solution, however, can not be expected. Crisfield [43] and Simo [49] suggested that a symmetric tangent stiffness matrix could be achieved if a certain set of additive rotational variables were employed in a co-rotational element formulation. Battini and Pacoste [55-56] parameterized the global rotations based on the Euler parameters (quaternion) [44], and obtained additive rotation variables, and thus symmetric tangent stiffness matrix. Ibrahimbegovic *et al*. [9] proposed a vector-like parameterization of three-dimensional finite rotation expressed through the well-known Rodrigues formula [6,44,57]. Even though these rotation parameters are additive, and lead to symmetric tangent stiffness, they are, however, not valid globally due to singularities that require additional treatments. To eliminate the singularities of the vector-like parameterization and the associated ill-conditioning problem, Ibrahimbegovic [10] employed incremental vector-like rotation parameters by restricting the size of the incremental rotation, where the finite rotations in each increment are updated by an iterative procedure, in which the material form of the incremental rotation vector is first updated by adding its iterative increment to the incremental rotation vector. The total spatial rotation is next obtained from its updated material representation by making use of the exponential mapping.

Compared with other existing co-rotational element formulations, the present curved 9-node quadrilateral shell element formulation has several features:

1) The vectorial rotational variables are defined as components of polar vectors, and thus all nodal variables (displacements and rotations) in the global coordinate system are additive in an

incremental nonlinear solution procedure;

2) All nodal variables are commutative in calculating the second derivatives of the element strain energy with respect to local nodal variables to obtain the local element tangent stiffness matrix and the local variables with respect to the global nodal variables to obtain the transformation matrix from local to global coordinate systems, resulting in symmetric element tangent stiffness matrices in the local and global coordinate systems;

3) The element tangent stiffness matrix and the transformation matrix from the local to global coordinate systems are updated using the total values of the nodal variables in an incremental solution procedure, making it advantageous for solving dynamic problems [58-59].

To verify the reliability and computational accuracy of the present 9-node co-rotational curved quadrilateral shell element, one smooth shell and six non-smooth plate/shell problems with large displacement and large rotation [60-63] are analyzed.

The outline of the paper is as follows. Section 2 presents the co-rotational framework defined for the 9-node curved quadrilateral shell element and the element kinematics. Section 3 describes the local and global element formulations, and the assumed strain procedure used to alleviate locking problems. Section 4 describes the treatment of special load and boundary conditions. Section 5 introduces the nonlinear solution procedure adopted in solving the following examples. In Section 6, one smooth shell and six folded or multi-plates/shells problems undergoing large displacements and large rotations are analyzed to demonstrate the reliability and computational accuracy of the proposed element formulation. Concluding remarks are presented in Section 7.

2. Kinematics

The Reissner-Mindlin theory is adopted in the present shell element. Only rigid junctions at the intersection of folded and multi-shell structures are considered. The intersections of irregular shell structures are treated as curved lines with the mid-surfaces of different shell patches interconnected non-smoothly. A co-rotational approach is used to exclude the influence of element rigid-body rotations from the local displacement field, leading to an element-independent formulation.

2.1. Co-rotational framework

In Figure 1, XYZ defines the global coordinate system, while *xyz* defines the local co-rotational system which rotates rigidly with the element as it deforms. The *x* and *y* axes of the local coordinate system are defined to be coincident with the bisectors of the diagonal vectors generated from the four corner nodes [34], while the local *z* axis is defined as orthogonal to the *x*-*y* axes.

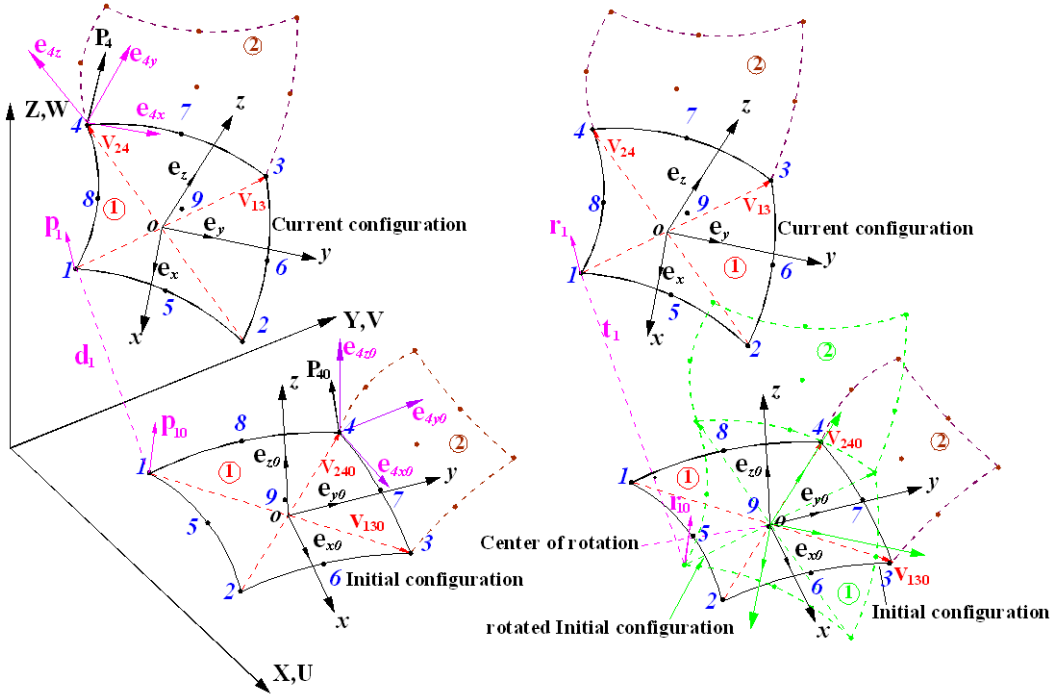

Figure 1. Definition of co-rotation framework and nodal orientation matrix

The co-rotational system at the initial configuration is defined by the orientation vectors $\mathbf{v}_{130}$ and $\mathbf{v}_{240}$, as obtained from:

$$\mathbf{v}_{130} = \mathbf{X}_{30} - \mathbf{X}_{10}; \qquad \mathbf{v}_{240} = \mathbf{X}_{40} - \mathbf{X}_{20} \tag{1a,b}$$

where $\mathbf{X}_{i0}$ is the global co-ordinates of Node *i* in the initial configuration.

The corresponding normalized unit vectors of ($\mathbf{v}_{130}$, $\mathbf{v}_{240}$)---called the "cross" vectors, each in the direction of a pair of opposite corner nodes---- are defined by:

$$\mathbf{c}_{130} = \frac{\mathbf{v}_{130}}{|\mathbf{v}_{130}|}; \qquad \mathbf{c}_{240} = \frac{\mathbf{v}_{240}}{|\mathbf{v}_{240}|} \tag{2a,b}$$

With the adopted definition of the local system, the initial triad vectors ($\mathbf{e}_{x0}$, $\mathbf{e}_{y0}$, $\mathbf{e}_{z0}$) of the local

co-rotational system are therefore determined as [34]:

$$\mathbf{e}_{x0} = \frac{\mathbf{c}_{130} - \mathbf{c}_{240}}{\left|\mathbf{c}_{130} - \mathbf{c}_{240}\right|}; \qquad \mathbf{e}_{y0} = \frac{\mathbf{c}_{130} + \mathbf{c}_{240}}{\left|\mathbf{c}_{130} + \mathbf{c}_{240}\right|}; \qquad \mathbf{e}_{z0} = \mathbf{e}_{x0} \times \mathbf{e}_{y0} \tag{3a,b,c}$$

We note here that defining the pair of orthogonal vectors $(\mathbf{e}_{x0}, \mathbf{e}_{y0})$ along the bisectors of the "cross" vectors $(\mathbf{c}_{130}, \mathbf{c}_{240})$ [64] is similar to the method in Hughes and Liu [65-66], Hughes [67], and Belytschko *et al.* [68, p.569, Eq.(9.5.16)].[1] Similarly, in the deformed configuration, the co-rotational framework is defined by the orientation vectors ($\mathbf{v}_{13}$, $\mathbf{v}_{24}$):

$$\mathbf{v}_{13} = \mathbf{v}_{130} + \mathbf{d}_3 - \mathbf{d}_1; \qquad \mathbf{v}_{24} = \mathbf{v}_{240} + \mathbf{d}_4 - \mathbf{d}_2 \tag{4a,b}$$

where $\mathbf{d}_i$ is the translational global displacement vector of Node i in the global coordinate system, with $\mathbf{d}_i^{\mathrm{T}} = \langle U_i \; V_i \; W_i \rangle$.

The corresponding unit vectors are determined from:

$$\mathbf{c}_{13} = \frac{\mathbf{v}_{13}}{\left|\mathbf{v}_{13}\right|}; \qquad \mathbf{c}_{24} = \frac{\mathbf{v}_{24}}{\left|\mathbf{v}_{24}\right|} \tag{5a,b}$$

leading to the triad ($\mathbf{e}_x$, $\mathbf{e}_y$, $\mathbf{e}_z$) of the co-rotational system in the deformed configuration:

$$\mathbf{e}_x = \frac{\mathbf{c}_{13} - \mathbf{c}_{24}}{\left|\mathbf{c}_{13} - \mathbf{c}_{24}\right|}; \qquad \mathbf{e}_y = \frac{\mathbf{c}_{13} + \mathbf{c}_{24}}{\left|\mathbf{c}_{13} + \mathbf{c}_{24}\right|}; \qquad \mathbf{e}_z = \mathbf{e}_x \times \mathbf{e}_y \tag{6a,b,c}$$

In the global system, the element employs either five or six degrees of freedom at each node, depending on the type of node:

$$\mathbf{u}_G^{\mathrm{T}} = \left\langle \mathbf{d}_1^{\mathrm{T}} \quad \mathbf{n}_{g1}^{\mathrm{T}} \quad \cdots \quad \mathbf{d}_i^{\mathrm{T}} \quad \mathbf{n}_{gi}^{\mathrm{T}} \quad \cdots \quad \mathbf{d}_9^{\mathrm{T}} \quad \mathbf{n}_{g9}^{\mathrm{T}} \right\rangle \tag{7}$$

At every node, there are three global nodal translational degrees of freedom contained in the matrix

---

[1] The difference is that the local coordinate system here is defined for the entire element, whereas the local coordinate system in Belytschko *et al.* [68, p.568, Eq.(9.5.13)] is based on two tangent vectors to the two coordinate lines in a shell lamina (a surface within a shell, at a constant transverse coordinate), and is pointwise, i.e., at a specific point within the shell lamina.

$\mathbf{d}_i^{\mathrm{T}} = \langle U_i \quad V_i \quad W_i \rangle$. At a node away from a shell intersection, there are two vectorial rotational degrees of freedom in $\mathbf{n}_{gi}^{\mathrm{T}} = \langle p_{i,n} \quad p_{i,m} \rangle$, where ($p_{i,n}$, $p_{i,m}$) are the two smallest global components of the nodal normal vector $\mathbf{p}_i$. At a node on the intersection of non-smooth shell, there are three vectorial rotational degrees of freedom in $\mathbf{n}_{gi}^{\mathrm{T}} = \langle e_{iy,n} \quad e_{iy,m} \quad e_{iz,n} \rangle$, where $|e_{iy,l}| \geq |e_{iy,m}|$, $|e_{iy,l}| \geq |e_{iy,n}|$ and $|e_{iz,m}| \geq |e_{iz,n}|$, with {*n*,*m*,*l*} being circular permutation of {*X*, *Y*, *Z*}, are assumed at the preceding incremental loading step to keep the signs of $e_{iy,l}$ and $e_{iz,m}$ unchanged at the present incremental loading step. The value of *n*, *m* and *l* may be different at different node, and may change at different incremental step in an incremental solution procedure. In other words, $e_{iy,m}$ and $e_{iy,n}$ are the two smallest components of vector $\mathbf{e}_{iy}$ at Node *i*, whereas $e_{iz,n}$ is the smallest, or next to smallest, component of vector $\mathbf{e}_{iz}$ at Node *i*.

Three other components of $\mathbf{e}_{iy}$ and $\mathbf{e}_{iz}$ can be calculated from ($e_{iy,n}$, $e_{iy,m}$, $e_{iz,n}$) at the present incremental loading step as follows

$$\| \mathbf{e}_{iy} \|^2 = e_{iy,l}^2 + e_{iy,m}^2 + e_{iy,n}^2 = 1 \Rightarrow e_{iy,l} = s_1 \sqrt{1 - (e_{iy,m}^2 + e_{iy,n}^2)} \tag{8a}$$

$$\| \mathbf{e}_{iz} \|^2 = e_{iz,l}^2 + e_{iz,m}^2 + e_{iz,n}^2 = 1 \Rightarrow e_{iz,m} = s_3 \sqrt{1 - (e_{iz,n}^2 + e_{iz,l}^2)} \tag{8b}$$

$$\left. \begin{array}{l} \left\| \mathbf{e}_{iy} \right\|^2 = 1 \\ \left\| \mathbf{e}_{iz} \right\|^2 = 1 \\ \mathbf{e}_{iy}^{\mathrm{T}} \mathbf{e}_{iz} = 0 \end{array} \right\} \Rightarrow e_{iz,l} = \frac{-e_{iy,l} e_{iy,n} e_{iz,n} + s_2 e_{iy,m} \sqrt{1 - e_{iy,n}^2 - e_{iz,n}^2}}{1 - e_{iy,n}^2} \tag{8c}$$

where the sign symbols (s_1 , s_3) take numerical value 1 or –1, and have the same signs as those of the components $e_{iy,l}$ and $e_{iz,m}$, respectively, in last incremental step, and $s_2 = -s_1 \cdot s_3$.

Vector $\mathbf{e}_{ix}$ is the cross-product of Vector $\mathbf{e}_{iy}$ and Vector $\mathbf{e}_{iz}$,

$$\mathbf{e}_{ix} = \mathbf{e}_{iy} \times \mathbf{e}_{iz} \tag{9}$$

In the local coordinate system, the element has 45 degrees of freedom:

$$\mathbf{u}_L^{\mathrm{T}} = \langle \mathbf{t}_1^{\mathrm{T}} \quad \boldsymbol{\theta}_1^{\mathrm{T}} \quad \cdots \quad \mathbf{t}_i^{\mathrm{T}} \quad \boldsymbol{\theta}_i^{\mathrm{T}} \quad \cdots \quad \mathbf{t}_9^{\mathrm{T}} \quad \boldsymbol{\theta}_9^{\mathrm{T}} \rangle \tag{10}$$

where $\mathbf{t}_i^{\mathrm{T}} = \langle u_i \ \upsilon_i \ w_i \rangle$ is the translational displacement vector of Node *i* in the local system, and $\boldsymbol{\theta}_i^{\mathrm{T}} = \langle r_{ix} \quad r_{iy} \rangle$ represents the two local components of the nodal normal vector $\mathbf{p}_i$ along the local x- and y-axes, respectively.

The relationship between the local and global nodal translational displacements is explicitly given by:

$$\mathbf{t}_i = \mathbf{R}\mathbf{d}_i + (\mathbf{R} - \mathbf{R}_0)\mathbf{v}_{i0} \qquad i = 1,2,\cdots,9 \tag{11}$$

where $\mathbf{R}_0$ and $\mathbf{R}$ are the orientation matrices of the co-rotational framework at the initial configuration and the current configuration, respectively, defined as:

$$\mathbf{R}_0{}^{\mathrm{T}} = \begin{bmatrix} \mathbf{e}_{x0} & \mathbf{e}_{y0} & \mathbf{e}_{z0} \end{bmatrix} \qquad \mathbf{R}^{\mathrm{T}} = \begin{bmatrix} \mathbf{e}_x & \mathbf{e}_y & \mathbf{e}_z \end{bmatrix} \tag{12}$$

with

$$\mathbf{v}_{i0} = \mathbf{X}_{i0} - \mathbf{X}_{90}, \ \ i = 1,2,\cdots,9 \tag{13}$$

representing a vector oriented from Node 9 to Node *i*.

In transforming the global nodal displacements to local nodal displacement according to Eq.(11), the initial local reference system is first rotated about Node 9 to the same orientation of the current reference system, though the centre of rotation is actually unimportant, and the local translations excluding rigid body rotation are measured from the initially rotated configuration, as illustrated in Figure 1.

The relationship between the local components and the global components of the nodal normal vector of mid-surface at a node away from the intersection of shell are obtained from:

$$\mathbf{r}_{i0} = \mathbf{R}_0\mathbf{p}_{i0} \tag{14a}$$

$$\mathbf{r}_i = \mathbf{R}\mathbf{p}_i \tag{14b}$$

where $\mathbf{p}_{i0}$ and $\mathbf{p}_i$ are the initial and current global components of the nodal normal vector at Node *i*, respectively; $\mathbf{r}_{i0}$ and $\mathbf{r}_i$ contain the initial and current local components of the nodal normal vector at Node *i*, respectively.

With the two smallest global components of the normal vector $\mathbf{p}_i$ used as vectorial rotational degrees of freedom at Node *i*, which is away from the intersection of shell mid-surface, the remaining component is obtained from:

$$p_{i,l} = s_4\sqrt{1 - p_{i,n}^2 - p_{i,m}^2} \qquad i = 1,2,\cdots,9 \tag{15}$$

where $s_4 = \pm 1$ takes the same sign as used for $p_{i,l}$ at the previous incremental step of load, and ($p_{i,n}$, $p_{i,m}$) represent the two smallest components of $\mathbf{p}_i$ used as global rotational degrees of freedom at Node *i*.

The relationship between the local components and the global components of the nodal normal vector of mid-surface at a node on the intersection of shell are obtained from:

$$\mathbf{r}_{i0} = \mathbf{R}_0\mathbf{p}_{i0} \tag{16a}$$

$$\mathbf{r}_i = \mathbf{R}\mathbf{R}_i^{\mathrm{T}}\mathbf{R}_{i0}\mathbf{p}_{i0} \tag{16b}$$

The orientation matrices $\mathbf{R}_{i0}$ and $\mathbf{R}_i$ of Node *i* on a shell intersection correspond to the initial configuration and current configuration, with

$$\mathbf{R}_{i0}^{\mathrm{T}} = \begin{bmatrix}\mathbf{e}_{ix0} & \mathbf{e}_{iy0} & \mathbf{e}_{iz0}\end{bmatrix} \tag{17a}$$

$$\mathbf{R}_i^{\mathrm{T}} = \begin{bmatrix}\mathbf{e}_{ix} & \mathbf{e}_{iy} & \mathbf{e}_{iz}\end{bmatrix} \tag{17b}$$

For convenience, the initial orientation matrix $\mathbf{R}_{i0}$ is defined as being coincident to the orientation matrix of the global coordinate system, i.e.,

$$\mathbf{e}_{ix0}^{\mathrm{T}} = \begin{Bmatrix}1 & 0 & 0\end{Bmatrix} \tag{18a}$$

$$\mathbf{e}_{iy0}^{\mathrm{T}} = \begin{Bmatrix}0 & 1 & 0\end{Bmatrix} \tag{18b}$$

$$\mathbf{e}_{iz0}^{\mathrm{T}} = \begin{Bmatrix}0 & 0 & 1\end{Bmatrix} \tag{18c}$$

and the triad of current orientation matrix $\mathbf{R}_i$ is evaluated from three nodal rotational variables as Eqs.(8a-c) and Eq.(9).

2.2. Evaluating mid-surface normal vector of smooth and non-smooth shell

Lagrangian interpolation functions are adopted to describe the geometry and the displacement field of the 9-node curved quadrilateral shell element:

$$h_i(\xi,\eta)=\frac{(\xi-\xi_j)(\xi-\xi_k)}{(\xi_l-\xi_j)(\xi_l-\xi_k)}\frac{(\eta-\eta_J)(\eta-\eta_K)}{(\eta_L-\eta_J)(\eta_L-\eta_K)} \quad i=1,2,\cdots,9 \tag{19}$$

where (ξ_l,η_L) represent the natural co-ordinates of Node i, with $\xi_j\neq\xi_k\neq\xi_l$ and $\eta_J\neq\eta_K\neq\eta_L$ representing the natural co-ordinates of the remaining nodes.

In the initial configuration, the local coordinates at any point within the element are obtained as:

$$\mathbf{x}=\sum h_i(\xi,\eta)\mathbf{x}_{i0}+\frac{1}{2}\zeta a h_i(\xi,\eta)\mathbf{r}_{i0} \tag{20}$$

where ζ is the natural co-ordinate in the direction of the element thickness, $\mathbf{r}_{i0}$ the initial normal vector at Node *i* in the local coordinate system, and *a* the thickness of element.

The local coordinates of Node i, required in Eq.(20), can be obtained from the corresponding nodal coordinates in the global coordinate system as:

$$\mathbf{x}_{i0}=\mathbf{R}_0\mathbf{v}_{i0} \tag{21}$$

The same Lagrangian shape functions are used to interpolate the translational and rotational fields, leading to an isoparametric formulation:

$$\mathbf{t}=\sum h_i(\xi,\eta)\mathbf{t}_i \tag{22}$$

$$\bar{\mathbf{r}}_h=\sum h_i(\xi,\eta)\boldsymbol{\theta}_i \tag{23}$$

where **t** is the vector of local translational fields, and $\bar{\mathbf{r}}_h$ the vector of local rotational fields.

The global components of the initial normal vector at Node *i* of the curved shell element are obtained from the cross-product of the tangent lines corresponding to independent variation in the two natural coordinates:

$$\bar{\mathbf{p}}_{i0}=\bar{\mathbf{X}}_{0,\xi}\times\bar{\mathbf{X}}_{0,\eta}\Big|_{(\xi_i,\eta_i)} \qquad i=1,2,\cdots,9 \tag{24}$$

where

$$\overline{\mathbf{X}}_0 = \sum_{j=1}^{9} h_j(\xi,\eta)\mathbf{X}_{j0}$$

with $\mathbf{X}_{j0}$ representing the global co-ordinates of Node *j*.

To minimize any discontinuity of slope between adjacent elements at Node i, due to the parametric definition of the element shape in terms of nodal co-ordinates with polynomial functions, the mean value of the normal vectors from the surrounding elements within the same piece of smooth shell is adopted:

$$\mathbf{p}_{i0} = \frac{\sum \overline{\mathbf{p}}_{i0} \Big/ \left|\overline{\mathbf{p}}_{i0}\right|}{\left|\sum \overline{\mathbf{p}}_{i0} \Big/ \left|\overline{\mathbf{p}}_{i0}\right|\right|} \qquad i = 1,2,\cdots,9 \tag{25}$$

On the other hand, if the true mid-surface of the curved shell is not smooth along the inter-element edges, the normal vector of element at node *i* shared by multiple elements within different adjacent pieces of smooth shell must be obtained independently, and three global rotational degrees of freedom would then be required for each node along the edges of the slope discontinuity. The normal vector of element at node *i* in the current configuration is updated as follows:

$$\mathbf{p}_i = \mathbf{R}_i^{\mathrm{T}} \mathbf{R}_{i0} \mathbf{p}_{i0} \tag{26}$$

where the rotation matrices $\mathbf{R}_{i0}$ and $\mathbf{R}_i$ correspond respectively to the initial orientation and the current orientation of Node *i* at the inter-element edge of non-smooth shell, as presented in Eqs.(8a-c), (9), (17a-b) and (18a-c).

3. Local and Global Element Formulations

The total potential energy of the 9-node curved quadrilateral shell element is calculated from,

$$\Pi = \frac{1}{2}\int_{\mathrm{V}} \boldsymbol{\varepsilon}^{\mathrm{T}} \mathbf{D}_1 \boldsymbol{\varepsilon}\, \mathrm{dV} + \frac{1}{2}\int_{\mathrm{V}} \boldsymbol{\gamma}^{T} \mathbf{D}_2 \boldsymbol{\gamma}\, \mathrm{dV} - \mathrm{W}_e \tag{27}$$

where Π is the total potential energy function, $\boldsymbol{\varepsilon}$ the in-plane strain vector, $\boldsymbol{\gamma}$ the transverse

shear strain vector, V the volume of the element, W_e the work done by external forces, with $\mathbf{D}_1$ and $\mathbf{D}_2$ being the elastic-moduli matrices,

$$\mathbf{D}_1 = \frac{\mathrm{E}}{1-\mu^2}\begin{bmatrix} 1 & \mu & 0 \\ \mu & 1 & 0 \\ 0 & 0 & \dfrac{1+\mu}{2} \end{bmatrix}; \qquad \mathbf{D}_2 = k_1 \frac{\mathrm{E}}{2(1+\mu)}\begin{bmatrix} 1 & 0 \\ 0 & 1 \end{bmatrix} \tag{28a,b}$$

where k_1 is the shear factor, and $k_1 = \dfrac{5}{6}$ or $k_1 = \dfrac{\pi^2}{12}$, E the Young's modulus, and μ the Poisson's ratio.

The Green-Lagrange strains specialized for shallow curved shell [43] are adopted in calculating the element strain energy. For convenience, the in-plane strain vector $\boldsymbol{\varepsilon}$ is split into two parts, a membrane strain vector $\boldsymbol{\varepsilon}_m$ and a bending strain vector $z_l\boldsymbol{\chi}$, resulting in Eq.(27) being rewritten as

$$\Pi = \frac{1}{2}\int_{\mathrm{V}} \left(\boldsymbol{\varepsilon}_m + z_l\boldsymbol{\chi}\right)^{\mathrm{T}} \mathbf{D}_1 \left(\boldsymbol{\varepsilon}_m + z_l\boldsymbol{\chi}\right)\mathrm{dV} + \frac{1}{2}\int_{\mathrm{V}} \boldsymbol{\gamma}^T \mathbf{D}_2 \boldsymbol{\gamma}\,\mathrm{dV} - \mathrm{W}_e \tag{29}$$

where

$$\boldsymbol{\varepsilon}_m = \begin{Bmatrix} \varepsilon_{xx} \\ \varepsilon_{yy} \\ \gamma_{xy} \end{Bmatrix} = \begin{Bmatrix} \dfrac{\partial \overline{u}}{\partial x} + \dfrac{1}{2}\left[\dfrac{\partial(\overline{w}+\overline{z}_0)}{\partial x}\right]^2 - \dfrac{1}{2}\left(\dfrac{\partial \overline{z}_0}{\partial x}\right)^2 \\ \dfrac{\partial \overline{\upsilon}}{\partial y} + \dfrac{1}{2}\left[\dfrac{\partial(\overline{w}+\overline{z}_0)}{\partial y}\right]^2 - \dfrac{1}{2}\left(\dfrac{\partial \overline{z}_0}{\partial y}\right)^2 \\ \dfrac{\partial \overline{u}}{\partial y} + \dfrac{\partial \overline{\upsilon}}{\partial x} + \dfrac{\partial(\overline{w}+\overline{z}_0)}{\partial x}\dfrac{\partial(\overline{w}+\overline{z}_0)}{\partial y} - \dfrac{\partial \overline{z}_0}{\partial x}\dfrac{\partial \overline{z}_0}{\partial y} \end{Bmatrix} \qquad z_l = \frac{1}{2}\zeta a \tag{30a}$$

$$\boldsymbol{\chi}^{\mathrm{T}} = \left\langle \frac{\partial\left(\overline{r}_x - \overline{r}_{x0}\right)}{\partial x}, \frac{\partial\left(\overline{r}_y - \overline{r}_{y0}\right)}{\partial y}, \frac{\partial\left(\overline{r}_x - \overline{r}_{x0}\right)}{\partial y} + \frac{\partial\left(\overline{r}_y - \overline{r}_{y0}\right)}{\partial x} \right\rangle \tag{30b}$$

$$\boldsymbol{\gamma} = \begin{Bmatrix} \gamma_{xz} \\ \gamma_{yz} \end{Bmatrix} = \begin{Bmatrix} \overline{r}_x - \overline{r}_{x0} + \dfrac{\partial w}{\partial x} \\ \overline{r}_y - \overline{r}_{y0} + \dfrac{\partial w}{\partial y} \end{Bmatrix} \tag{30c}$$

with $\bar{r}_x = \sum_{i=1}^{9} h_i r_{ix}$; $\bar{r}_{x0} = \sum_{i=1}^{9} h_i r_{ix0}$; $\bar{r}_y = \sum_{i=1}^{9} h_i r_{iy}$; $\bar{r}_{y0} = \sum_{i=1}^{9} h_i r_{iy0}$; $\bar{u} = \sum_{i=1}^{9} h_i u_i$;

$\bar{v} = \sum_{i=1}^{9} h_i v_i$; $\bar{w} = \sum_{i=1}^{9} h_i w_i$; $\bar{z}_0 = \sum_{i=1}^{9} h_i z_{i0}$.

The derivatives of the nodal variables with respect to the local coordinates can be calculated from

$$\begin{Bmatrix} \frac{\partial}{\partial x} \\ \frac{\partial}{\partial y} \\ \frac{\partial}{\partial z} \end{Bmatrix} = \mathbf{J}^{-1} \begin{Bmatrix} \frac{\partial}{\partial \xi} \\ \frac{\partial}{\partial \eta} \\ \frac{\partial}{\partial \zeta} \end{Bmatrix}; \qquad \mathbf{J} = \begin{bmatrix} \frac{\partial x}{\partial \xi} & \frac{\partial y}{\partial \xi} & \frac{\partial z}{\partial \xi} \\ \frac{\partial x}{\partial \eta} & \frac{\partial y}{\partial \eta} & \frac{\partial z}{\partial \eta} \\ \frac{\partial x}{\partial \zeta} & \frac{\partial y}{\partial \zeta} & \frac{\partial z}{\partial \zeta} \end{bmatrix} \tag{31a,b}$$

The variation of the potential energy of the element with respect to the local nodal variables is given by

$$\delta\Pi = [\int_{\mathrm{V}} (\boldsymbol{\varepsilon}_m + z_l \boldsymbol{\chi})^{\mathrm{T}} \mathbf{D}_1 (\mathbf{B}_m + z_l \mathbf{B}_b) \mathrm{dV} + \int_{\mathrm{V}} \boldsymbol{\gamma}^T \mathbf{D}_2 \mathbf{B}_\gamma \, \mathrm{dV}] \delta \mathbf{u}_L - \mathbf{f}_{ext} \delta \bar{\mathbf{u}} = 0 \tag{32}$$

Where the matrices $\mathbf{B}_m$, $z_l \mathbf{B}_b$, and $\mathbf{B}_\gamma$ are respectively the first derivatives of the membrane strain vector $\boldsymbol{\varepsilon}_m$, the bending strain vector $z_l \boldsymbol{\chi}$, and the out-of-plane shear strain vector $\boldsymbol{\gamma}$ with respect to the local nodal variable vector. The expressions of these derivatives are given in Appendix A.

The internal force vector in the local coordinate system is given by

$$\begin{aligned} \mathbf{f} = \mathbf{f}_{ext} &= \int_{\mathrm{V}} (\mathbf{B}_m + z_l \mathbf{B}_b)^{\mathrm{T}} \mathbf{D}_1 (\boldsymbol{\varepsilon}_m + z_l \boldsymbol{\chi}) \mathrm{dV} + \int_{\mathrm{V}} \mathbf{B}_\gamma^{\mathrm{T}} \mathbf{D}_2 \boldsymbol{\gamma} \, \mathrm{dV} \\ &= \int_{\mathrm{V}} [\mathbf{B}_m^{\mathrm{T}} \mathbf{D}_1 \boldsymbol{\varepsilon}_m + (z_l)^2 \mathbf{B}_b^{\mathrm{T}} \mathbf{D}_1 \boldsymbol{\chi}] \mathrm{dV} + \int_{\mathrm{V}} \mathbf{B}_\gamma^{\mathrm{T}} \mathbf{D}_2 \boldsymbol{\gamma} \, \mathrm{dV} \end{aligned} \tag{33}$$

By differentiating the internal force vector with respect to the local nodal variables, the tangent stiffness matrix of the 9-node curved quadrilateral shell element is obtained

$$\mathbf{k}_T = \int_{\mathrm{V}} [\mathbf{B}_m^{\mathbf{T}} \mathbf{D}_1 \mathbf{B}_m + (z_l)^2 \mathbf{B}_b^{\mathbf{T}} \mathbf{D}_1 \mathbf{B}_b + \frac{\partial \mathbf{B}_m^{\mathbf{T}}}{\partial \mathbf{u}_L^{\mathrm{T}}} \mathbf{D}_1 \boldsymbol{\varepsilon}_m + \mathbf{B}_\gamma^{\mathbf{T}} \mathbf{D}_2 \mathbf{B}_\gamma] \mathrm{dV} \tag{34}$$

where $\frac{\partial \mathbf{B}_m}{\partial \mathbf{u}_L^{\mathrm{T}}}$ is the second derivative of the membrane strain vector $\boldsymbol{\varepsilon}_m$ with respect to the local nodal variable vector; see the details in Appendix A.

Eq.(33) and Eq.(34) are the conforming element formulations for the 9-node curved quadrilateral shell element in the local coordinate system. Due to the commutativity of the local nodal variables in calculating the second derivatives of the potential functional Π, the resulting element tangent stiffness matrix $\mathbf{k}_T$ is symmetric.

In solving thin-shell problems, the membrane and shear locking phenomena will not only lead to inaccurate results, but also deteriorate the convergence and the computational efficiency of the element formulations. To improve the performance of the present curved quadrilateral shell element formulation, the membrane strains, the out-of-plane shear strains, and their first and second derivatives with respect to the local nodal variables are replaced, respectively, with assumed strains and their derivatives with respect to the local nodal variables. The improved element formulations are then given as follows

$$\mathbf{f} = \int_{\mathrm{V}} [\tilde{\mathbf{B}}_m^{\mathrm{T}} \mathbf{D}_1 \tilde{\boldsymbol{\varepsilon}}_m + (z_l)^2 \mathbf{B}_b^{\mathrm{T}} \mathbf{D}_1 \boldsymbol{\chi}] \mathrm{dV} + \int_{\mathrm{V}} \tilde{\mathbf{B}}_\gamma^{\mathrm{T}} \mathbf{D}_2 \tilde{\boldsymbol{\gamma}} \, \mathrm{dV} \tag{35}$$

$$\mathbf{k}_T = \int_{\mathrm{V}} [\tilde{\mathbf{B}}_m^{\mathrm{T}} \mathbf{D}_1 \tilde{\mathbf{B}}_m + (z_l)^2 \mathbf{B}_b^{\mathrm{T}} \mathbf{D}_1 \mathbf{B}_b + \frac{\partial \tilde{\mathbf{B}}_m^{\mathrm{T}}}{\partial \mathbf{u}_L^{\mathrm{T}}} \mathbf{D}_1 \tilde{\boldsymbol{\varepsilon}}_m + \tilde{\mathbf{B}}_\gamma^{\mathrm{T}} \mathbf{D}_2 \tilde{\mathbf{B}}_\gamma] \mathrm{dV} \tag{36}$$

where

$$\tilde{\boldsymbol{\varepsilon}}_m^{\mathrm{T}} = \left\langle \tilde{\varepsilon}_{xx} \quad \tilde{\varepsilon}_{yy} \quad \tilde{\gamma}_{xy} \right\rangle \quad , \qquad \tilde{\boldsymbol{\gamma}}^{\mathrm{T}} = \left\langle \tilde{\gamma}_{xz} \quad \tilde{\gamma}_{yz} \right\rangle \quad , \quad \tilde{\mathbf{B}}_m = \begin{Bmatrix} \tilde{\mathbf{B}}_{xx} \\ \tilde{\mathbf{B}}_{yy} \\ \tilde{\mathbf{B}}_{xy} \end{Bmatrix} \quad , \qquad \tilde{\mathbf{B}}_\gamma = \begin{Bmatrix} \tilde{\mathbf{B}}_{xz} \\ \tilde{\mathbf{B}}_{yz} \end{Bmatrix} \quad ,$$

$$\frac{\partial \tilde{\mathbf{B}}_m}{\partial \mathbf{u}_L^{\mathrm{T}}} = \begin{Bmatrix} \frac{\partial \tilde{\mathbf{B}}_{xx}}{\partial \mathbf{u}_L^{\mathrm{T}}} \\ \frac{\partial \tilde{\mathbf{B}}_{yy}}{\partial \mathbf{u}_L^{\mathrm{T}}} \\ \frac{\partial \tilde{\mathbf{B}}_{xy}}{\partial \mathbf{u}_L^{\mathrm{T}}} \end{Bmatrix}$$

The Mixed Interpolation of Tensorial Components (MITC) approach [41] is employed in calculating the assumed strains by replacing the membrane strain and out-of-plane shear strain

components in natural coordinates with the membrane strains and the out-of-plane shear strains in Cartesian coordinates.

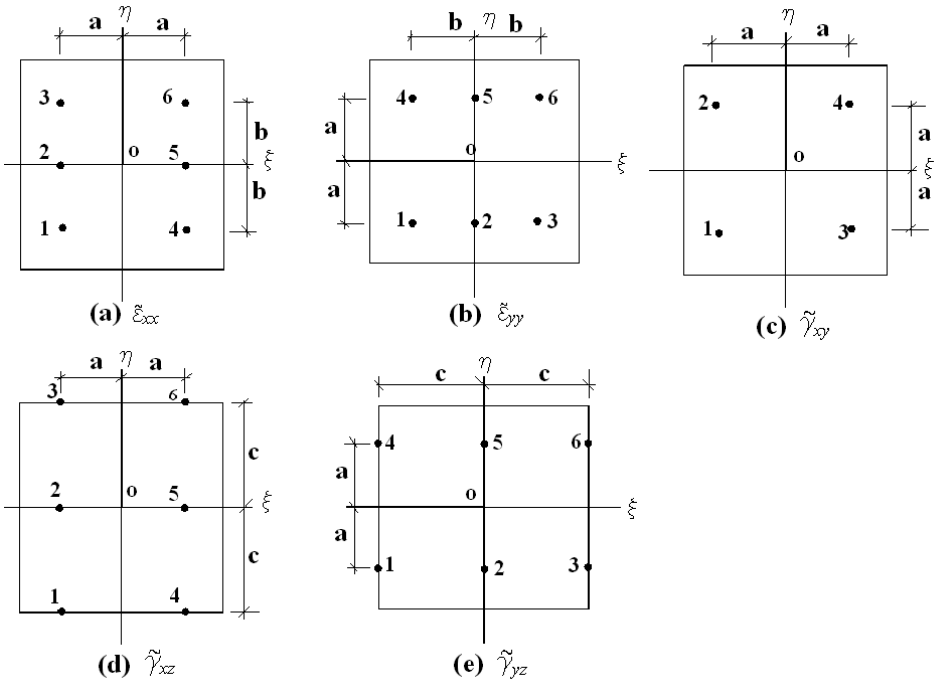

Figure 2. Tying positions of the curved quadrilateral shell element

The assumed strains are interpolated by using the conforming strains at the well-chosen tying points on the shell mid-surface (see Figures 2a-e),

$$\tilde{\varepsilon}_{xx}=\sum_{i=1}^{6}N_i\varepsilon_{ixx}\ ;\quad \tilde{\varepsilon}_{yy}=\sum_{i=1}^{6}N_i\varepsilon_{iyy}\ ;\quad \tilde{\gamma}_{xy}=\sum_{i=1}^{4}N_i\gamma_{ixy}\ ;\quad \tilde{\gamma}_{xz}=\sum_{i=1}^{6}N_i\gamma_{ixz}\ ;\quad \tilde{\gamma}_{yz}=\sum_{i=1}^{6}N_i\gamma_{iyz}$$

(37a-e)

where the first subscript i in the right side of the conforming strain ε_{ixx}, ε_{iyy}, γ_{ixy}, γ_{ixz} and γ_{iyz} represents the position of the tying point with natural coordinates (ξ_l,η_L). For the normal strain $\tilde{\varepsilon}_{xx}$ and transverse shear strain $\tilde{\gamma}_{xz}$, the interpolating functions are $N_i=\dfrac{(\xi-\xi_j)}{(\xi_l-\xi_j)}\dfrac{(\eta-\eta_J)(\eta-\eta_K)}{(\eta_L-\eta_J)(\eta_L-\eta_K)}$. For the in-plane shear strain $\tilde{\gamma}_{xy}$, the interpolating functions are $N_i=\dfrac{(\xi-\xi_j)}{(\xi_l-\xi_j)}\dfrac{(\eta-\eta_K)}{(\eta_L-\eta_K)}$. For the normal strain $\tilde{\varepsilon}_{yy}$ and transverse shear strain $\tilde{\gamma}_{yz}$, the

interpolating functions are $N_i = \dfrac{(\xi-\xi_j)(\xi-\xi_k)}{(\xi_l-\xi_j)(\xi_l-\xi_k)}\dfrac{(\eta-\eta_J)}{(\eta_L-\eta_J)}$. In these interpolation functions, $\xi_l \neq \xi_j \neq \xi_k$ and $\eta_L \neq \eta_J \neq \eta_K$ are the natural coordinates of the tying points, and take the values of 0, $\pm a$, $\pm b$ or $\pm c$, with $a = \dfrac{1}{\sqrt{3}}$, $b = \sqrt{\dfrac{3}{5}}$, $c = 1$.

After introducing the assumed strains, the resulting element tangent stiffness matrix is still symmetric.

The internal force vector $\mathbf{f}_g$ of the curved quadrilateral shell element in the global coordinate system can be calculated from that in the local coordinate system,

$$\mathbf{f}_g = \mathbf{T}^{\mathrm{T}}\mathbf{f} \tag{38}$$

where $\mathbf{T}^{\mathrm{T}}$ is the transpose of the transformation matrix $\mathbf{T}$, which can be calculated from the relationships of the nodal variables in the local and global coordinate systems as follows [see Eq.(11), Eqs.(14a,b), and Eqs.(16a,b)]

$$\mathbf{T} = \left[\frac{\partial u_{Li}}{\partial u_{Gj}}\right] = \begin{bmatrix} \dfrac{\partial \mathbf{t}_1}{\partial \mathbf{d}_1} & 0 & \cdots & \dfrac{\partial \mathbf{t}_1}{\partial \mathbf{d}_9} & 0 \\ \dfrac{\partial \boldsymbol{\theta}_1}{\partial \mathbf{d}_1} & \dfrac{\partial \boldsymbol{\theta}_1}{\partial \mathbf{n}_{g1}} & \cdots & \dfrac{\partial \boldsymbol{\theta}_1}{\partial \mathbf{d}_9} & \dfrac{\partial \boldsymbol{\theta}_1}{\partial \mathbf{n}_{g9}} \\ \vdots & \vdots & \vdots & \vdots & \vdots \\ \dfrac{\partial \mathbf{t}_9}{\partial \mathbf{d}_1} & 0 & \cdots & \dfrac{\partial \mathbf{t}_9}{\partial \mathbf{d}_9} & 0 \\ \dfrac{\partial \boldsymbol{\theta}_9}{\partial \mathbf{d}_1} & \dfrac{\partial \boldsymbol{\theta}_9}{\partial \mathbf{n}_{g1}} & \cdots & \dfrac{\partial \boldsymbol{\theta}_9}{\partial \mathbf{d}_9} & \dfrac{\partial \boldsymbol{\theta}_9}{\partial \mathbf{n}_{g9}} \end{bmatrix} \tag{39}$$

with the details of the sub-matrices of $\mathbf{T}$ given in Appendix B.

The element tangent stiffness matrix $\mathbf{k}_{TG}$ in the global coordinate system is calculated by differentiating $\mathbf{f}_g$ with respect to the global nodal variable vector $\mathbf{u}_G$ to yield

$$\mathbf{k}_{TG} = \frac{\partial \mathbf{f}_g}{\partial \mathbf{u}_G^{\mathrm{T}}} = \mathbf{T}^{\mathrm{T}}\frac{\partial \mathbf{f}}{\partial \mathbf{u}_G^{\mathrm{T}}} + \frac{\partial \mathbf{T}^{\mathrm{T}}}{\partial \mathbf{u}_G^{\mathrm{T}}}\mathbf{f} = \mathbf{T}^{\mathrm{T}}\frac{\partial \mathbf{f}}{\partial \mathbf{u}_L^{\mathrm{T}}}\mathbf{T} + \frac{\partial \mathbf{T}^{\mathrm{T}}}{\partial \mathbf{u}_G^{\mathrm{T}}}\mathbf{f} = \mathbf{T}^{\mathrm{T}}\mathbf{k}_T\mathbf{T} + \frac{\partial \mathbf{T}^{\mathrm{T}}}{\partial \mathbf{u}_G^{\mathrm{T}}}\mathbf{f} \tag{40}$$

$$\frac{\partial \mathbf{T}}{\partial \mathbf{u}_G^{\mathrm{T}}}=\left[\frac{\partial^2 u_{Li}}{\partial u_{Gj}\partial u_{Gk}}\right]=\begin{bmatrix} \dfrac{\partial^2 \mathbf{t}_1}{\partial \mathbf{d}_1^{\mathrm{T}}\partial \mathbf{u}_G^{\mathrm{T}}} & 0 & \cdots & \dfrac{\partial^2 \mathbf{t}_1}{\partial \mathbf{d}_9^{\mathrm{T}}\partial \mathbf{u}_G^{\mathrm{T}}} & 0 \\ \dfrac{\partial^2 \boldsymbol{\theta}_1}{\partial \mathbf{d}_1^{\mathrm{T}}\partial \mathbf{u}_G^{\mathrm{T}}} & \dfrac{\partial^2 \boldsymbol{\theta}_1}{\partial \mathbf{n}_{g1}^{\mathrm{T}}\partial \mathbf{u}_G^{\mathrm{T}}} & \cdots & \dfrac{\partial^2 \boldsymbol{\theta}_1}{\partial \mathbf{d}_9^{\mathrm{T}}\partial \mathbf{u}_G^{\mathrm{T}}} & \dfrac{\partial^2 \boldsymbol{\theta}_1}{\partial \mathbf{n}_{g9}^{\mathrm{T}}\partial \mathbf{u}_G^{\mathrm{T}}} \\ \vdots & \vdots & \vdots & \vdots & \vdots \\ \dfrac{\partial^2 \mathbf{t}_9}{\partial \mathbf{d}_1^{\mathrm{T}}\partial \mathbf{u}_G^{\mathrm{T}}} & 0 & \cdots & \dfrac{\partial^2 \mathbf{t}_9}{\partial \mathbf{d}_9^{\mathrm{T}}\partial \mathbf{u}_G^{\mathrm{T}}} & 0 \\ \dfrac{\partial^2 \boldsymbol{\theta}_9}{\partial \mathbf{d}_1^{\mathrm{T}}\partial \mathbf{u}_G^{\mathrm{T}}} & \dfrac{\partial^2 \boldsymbol{\theta}_9}{\partial \mathbf{n}_{g1}^{\mathrm{T}}\partial \mathbf{u}_G^{\mathrm{T}}} & \cdots & \dfrac{\partial^2 \boldsymbol{\theta}_9}{\partial \mathbf{d}_9^{\mathrm{T}}\partial \mathbf{u}_G^{\mathrm{T}}} & \dfrac{\partial^2 \boldsymbol{\theta}_9}{\partial \mathbf{n}_{g9}^{\mathrm{T}}\partial \mathbf{u}_G^{\mathrm{T}}} \end{bmatrix} \tag{41}$$

with the details of the sub-matrices of $\dfrac{\partial \mathbf{T}}{\partial \mathbf{u}_G^{\mathrm{T}}}$ given in Appendix B. In the right side of Eq.(40), the first term is symmetric. Owing to the commutativity of the global nodal variables in the differentiation of Eq.(41), the second term of Eq.(40) is also symmetric, consequently leading to the element tangent stiffness matrix in the global coordinate system being symmetric.[2]

The derivation of the symmetry of the term $\dfrac{\partial \mathbf{T}^{\mathrm{T}}}{\partial \mathbf{u}_G^{\mathrm{T}}}\mathbf{f}$ in Eq.(40) begins with writing Eq.(39) with indices as follows,

$$\mathbf{T}=\left[T_{ij}\right]=\left[\frac{\partial u_{Li}}{\partial u_{Gj}}\right] \tag{42}$$

with the subscripts "*L*" and "*G*" meaning "Local" and "Global", respectively, whereas *i* is the row index and *j* the column index. Then the force $\mathbf{f}_g$ can be written with components as

$$\mathbf{f}_g=\mathbf{T}^{\mathrm{T}}\mathbf{f} \Rightarrow \left\{f_{gi}\right\}=\left\{T_{ki}\,f_k\right\}=\left\{\frac{\partial u_{Lk}}{\partial u_{Gi}}\,f_k\right\} \tag{43}$$

where the summation on the repeated index *k* was implied, and

$$\frac{\partial \mathbf{T}^{\mathrm{T}}}{\partial \mathbf{u}_G}\mathbf{f}=\left[\frac{\partial^2 u_{Lk}}{\partial u_{Gj}\partial u_{Gi}}\right]\left\{f_k\right\}=\left[\frac{\partial^2 u_{Lk}\,f_k}{\partial u_{Gj}\partial u_{Gi}}\right]=\left[\frac{\partial^2 u_{Lk}\,f_k}{\partial u_{Gi}\partial u_{Gj}}\right]=\left(\frac{\partial \mathbf{T}^{\mathrm{T}}}{\partial \mathbf{u}_G}\mathbf{f}\right)^{\mathrm{T}} \tag{44}$$

since

---

[2] While symmetry of the tangent stiffness matrix would be relevant for traditional finite-element codes it is not relevant for multibody-dynamics codes, in which both rigid bodies and flexible bodies can co-exist with complex connections among them, since all second-order ODEs are converted to first-order ODEs so many advanced Higher-Order Time INTegrators (HOTINT) can be used, resulting in non-symmetric "tangent-stiffness" matrix [71][72].

$$\frac{\partial^2 u_{Lk}}{\partial u_{Gj}\partial u_{Gi}} = \frac{\partial^2 u_{Lk}}{\partial u_{Gi}\partial u_{Gj}} \tag{45}$$

It follows that the second term $\frac{\partial \mathbf{T}^{\mathrm{T}}}{\partial \mathbf{u}_G}\mathbf{f}$ of Eq.(40) is symmetric.

4. Treatment of special load and boundary condition

Different from other existing co-rotational shell elements --- which use rotation axial vectors (pseudo-vectors) or the related spin tensors as degrees of freedom, leading to non-symmetric tangent matrix --- the present element formulation employs vectorial rotational variables that are components of polar (proper) vectors to develop a co-rotation framework for large displacement and large rotation problems. Any existing applied moments that correspond to the rotation axial vectors are transformed into equivalent loads for the corresponding vectorial rotation variables [70].

Assuming that vector $\mathbf{e}_n$ is rotated through infinitesimal rotations of $\delta\boldsymbol{\theta}^T = \langle \delta\theta_x \quad \delta\theta_y \quad \delta\theta_z \rangle$ to become vector $\mathbf{e}_{n+1}$, then an approximate relationship of $\mathbf{e}_n$ and $\mathbf{e}_{n+1}$ can be given as

$$\mathbf{e}_{n+1} = \mathbf{e}_n + \delta\boldsymbol{\theta} \times \mathbf{e}_n = [\mathbf{I} + \mathbf{S}(\delta\boldsymbol{\theta})]\mathbf{e}_n \tag{46}$$

where $\mathbf{I}$ is a 3×3 unit matrix, and $\mathbf{S}(\delta\boldsymbol{\theta})$ a skew-symmetric matrix of components of the corresponding spin tensor [44]

$$\mathbf{S}(\delta\boldsymbol{\theta}) = \begin{bmatrix} 0 & -\delta\theta_z & \delta\theta_y \\ \delta\theta_z & 0 & -\delta\theta_x \\ -\delta\theta_y & \delta\theta_x & 0 \end{bmatrix} \tag{47}$$

Eq.(46) can be rewritten as

$$\mathbf{e}_{n+1} - \mathbf{e}_n = \mathbf{S}(\delta\boldsymbol{\theta})\mathbf{e}_n = -\mathbf{S}(\mathbf{e}_n)\delta\boldsymbol{\theta} \tag{48}$$

or

$$\delta\mathbf{e}_n = -\mathbf{S}(\mathbf{e}_n)\delta\boldsymbol{\theta} \tag{49}$$

Thus the relationship between the orientation vectors $(\mathbf{e}_{iy}, \mathbf{e}_{iz})$ at Node *i* and the nodal axial rotation vector $\delta\boldsymbol{\theta}$ can be written as

$$\left.\begin{aligned}\delta\mathbf{e}_{iy} &= -\mathbf{S}(\mathbf{e}_{iy})\delta\boldsymbol{\theta}\\ \delta\mathbf{e}_{iz} &= -\mathbf{S}(\mathbf{e}_{iz})\delta\boldsymbol{\theta}\end{aligned}\right\} \tag{50}$$

Furthermore, the relationship between the incremental vectorial rotation variables and the nodal axial rotation variables can be given as

$$\begin{Bmatrix}\delta e_{iy,n}\\ \delta e_{iy,m}\\ \delta e_{iz,n}\end{Bmatrix} = -\begin{bmatrix}S_{n,1}(\mathbf{e}_{iy}) & S_{n,2}(\mathbf{e}_{iy}) & S_{n,3}(\mathbf{e}_{iy})\\ S_{m,1}(\mathbf{e}_{iy}) & S_{m,2}(\mathbf{e}_{iy}) & S_{m,3}(\mathbf{e}_{iy})\\ S_{n,1}(\mathbf{e}_{iz}) & S_{n,2}(\mathbf{e}_{iz}) & S_{n,3}(\mathbf{e}_{iz})\end{bmatrix}\begin{Bmatrix}\delta\theta_{ix}\\ \delta\theta_{iy}\\ \delta\theta_{iz}\end{Bmatrix} \tag{51}$$

where $S_{j,k}(\mathbf{e}_{iy})$ and $S_{j,k}(\mathbf{e}_{iz})$ are respectively the components of $\mathbf{S}(\mathbf{e}_{iy})$ and $\mathbf{S}(\mathbf{e}_{iz})$ at jth row and kth column.

In calculating the equivalent components of the external force vector with respect to vectorial rotation variables, the work done by the equivalent components must be equal to that done by the corresponding moments at Node i, that is,

$$\begin{Bmatrix}M_{eq1}\\ M_{eq2}\\ M_{eq3}\end{Bmatrix}^{\mathrm{T}}\begin{Bmatrix}\delta e_{iy,n}\\ \delta e_{iy,m}\\ \delta e_{iz,n}\end{Bmatrix} = \begin{Bmatrix}M_{ix}\\ M_{iy}\\ M_{iz}\end{Bmatrix}^{\mathrm{T}}\begin{Bmatrix}\delta\theta_{ix}\\ \delta\theta_{iy}\\ \delta\theta_{iz}\end{Bmatrix} \tag{52}$$

where M_{eqj} (j=1,2,3) are the equivalent components of the external force vector with respect to vectorial rotation variable, and $M_{i\alpha}$ ($\alpha = x, y, z$) the moment components applied at Node *i*.

Substitute Eq.(51) into Eq.(52), the equivalent components of the external force vector with respect to vectorial rotation variables can be calculated as

$$\begin{Bmatrix}M_{eq1}\\ M_{eq2}\\ M_{eq3}\end{Bmatrix} = -\begin{bmatrix}S_{n,1}(\mathbf{e}_{iy}) & S_{n,2}(\mathbf{e}_{iy}) & S_{n,3}(\mathbf{e}_{iy})\\ S_{m,1}(\mathbf{e}_{iy}) & S_{m,2}(\mathbf{e}_{iy}) & S_{m,3}(\mathbf{e}_{iy})\\ S_{n,1}(\mathbf{e}_{iz}) & S_{n,2}(\mathbf{e}_{iz}) & S_{n,3}(\mathbf{e}_{iz})\end{bmatrix}^{-\mathrm{T}}\begin{Bmatrix}M_{ix}\\ M_{iy}\\ M_{iz}\end{Bmatrix} \tag{53}$$

If the direction of a constraint of nodal displacement is not coincident with any axis of global coordinate system, a modification of the element tangent stiffness matrix $\mathbf{k}_{TG}$ is necessary. A new orientation matrix $\mathbf{R}_c$ is defined at the node with special constraint, part of its orientation vectors is selected to be coincident to the directions of constrained displacements, then a relationship between the constrained displacement $\mathbf{d}_{ci}$ and its components $\mathbf{d}_i$ in global coordinate system is established through the new orientation matrix

$$\mathbf{d}_{ci} = \mathbf{R}_c \mathbf{d}_i \quad \text{or} \quad \Delta\mathbf{d}_{ci} = \mathbf{R}_c \Delta\mathbf{d}_i \tag{54}$$

Similarly, the relation between the load components in the constraint directions and those in the directions of global coordinate axes is obtained as follows

$$\mathbf{P}_{ci} = \mathbf{R}_c \mathbf{P}_i \quad \text{or} \quad \Delta\mathbf{P}_{ci} = \mathbf{R}_c \Delta\mathbf{P}_i \tag{55}$$

In an incremental nonlinear solution procedure, substitute Eq.(54) and Eq.(55) into the element force-displacement relation in global coordinate system

$$\mathbf{k}_{TG} \Delta\mathbf{u}_G = \Delta\mathbf{P}_e \tag{56}$$

to obtain the force-displacement relation

$$\begin{bmatrix} {}^{A}\mathbf{k}_{TG} & {}^{B}\mathbf{k}_{TG} & {}^{C}\mathbf{k}_{TG} \\ {}^{B}\mathbf{k}_{TG}^{\mathrm{T}} & {}^{D}\mathbf{k}_{TG} & {}^{E}\mathbf{k}_{TG} \\ {}^{C}\mathbf{k}_{TG}^{\mathrm{T}} & {}^{E}\mathbf{k}_{TG}^{\mathrm{T}} & {}^{F}\mathbf{k}_{TG} \end{bmatrix} \begin{Bmatrix} \Delta\mathbf{u}_{G1} \\ \mathbf{R}_c^{\mathrm{T}} \Delta\mathbf{d}_{ci} \\ \Delta\mathbf{u}_{G3} \end{Bmatrix} = \begin{Bmatrix} \Delta\mathbf{P}_1 \\ \mathbf{R}_c^{\mathrm{T}} \Delta\mathbf{P}_{ci} \\ \Delta\mathbf{P}_3 \end{Bmatrix} \tag{57}$$

where, ${}^{\alpha}\mathbf{k}_{TG}$ ($\alpha = A, B, \cdots, F$) are the sub-matrices of $\mathbf{k}_{TG}$; the column matrices $\Delta\mathbf{u}_{G1}, \Delta\mathbf{d}_i$ and $\Delta\mathbf{u}_{G3}$ are the sub-matrices of $\Delta\mathbf{u}_G$; likewise, the column matrices $\Delta\mathbf{P}_1, \Delta\mathbf{P}_i$ and $\Delta\mathbf{P}_3$ are the sub-matrices of $\Delta\mathbf{P}_e$.

Using the orthogonality of the orientation matrix $\mathbf{R}_c$, Eq.(57) can be rewritten with the matrix $\mathbf{R}_c$ appearing in the tangent stiffness matrix as follows

$$\begin{bmatrix} {}^{A}\mathbf{k}_{TG} & {}^{B}\mathbf{k}_{TG}\mathbf{R}_c^{\mathrm{T}} & {}^{C}\mathbf{k}_{TG} \\ \mathbf{R}_c\,{}^{B}\mathbf{k}_{TG}^{\mathrm{T}} & \mathbf{R}_c\,{}^{D}\mathbf{k}_{TG}\mathbf{R}_c^{\mathrm{T}} & \mathbf{R}_c\,{}^{E}\mathbf{k}_{TG} \\ {}^{C}\mathbf{k}_{TG}^{\mathrm{T}} & {}^{E}\mathbf{k}_{TG}^{\mathrm{T}}\mathbf{R}_c^{\mathrm{T}} & {}^{F}\mathbf{k}_{TG} \end{bmatrix} \begin{Bmatrix} \Delta\mathbf{u}_{G1} \\ \Delta\mathbf{d}_{ci} \\ \Delta\mathbf{u}_{G3} \end{Bmatrix} = \begin{Bmatrix} \Delta\mathbf{P}_1 \\ \Delta\mathbf{P}_{ci} \\ \Delta\mathbf{P}_3 \end{Bmatrix} \tag{58}$$

The element tangent stiffness matrix expressed in Eq.(58) is then assembled into the global stiffness matrix, which incorporates the displacement constraints via the orientation matrix $\mathbf{R}_c$.

5. Nonlinear solution procedure

In the present nonlinear solution procedure, the incremental force-displacement relation at the start of the ith loading increment is given as follows

$$\mathbf{K}_0^i \Delta\mathbf{U}_1^i = \Delta\lambda_1^i \mathbf{P} \tag{59}$$

where $\mathbf{K}_0^i$ is the assembled global tangent stiffness matrix at the start of the incremental loading Step i; $\Delta\mathbf{U}_1^i$ the increment of the global variables; $\mathbf{P}$ the prescribed external force vector; and $\Delta\lambda_1^i$ the increment of the loading parameter, calculated in accordance with the general displacement control procedure [70]:

$$\Delta\lambda_1^i = (-1)^n \Delta\lambda_1^1 \left|GSP\right|^{\frac{1}{2}} \tag{60}$$

where GSP is the General Stiffness Parameter, with *n* being the number of times that the sign of GSP changes, and $\Delta\lambda_1^1$ a prescribed initial incremental loading parameter, which can be evaluated through an advanced trial. The GSP is calculated as follows

$$GSP = \frac{\mathbf{U}_{11}^{1\mathrm{T}}\mathbf{U}_{11}^{1}}{\mathbf{U}_{11}^{i-1\mathrm{T}}\mathbf{U}_{11}^{i}} \tag{61}$$

where the matrices $\mathbf{U}_{11}^{1}$, $\mathbf{U}_{11}^{i-1}$, and $\mathbf{U}_{11}^{i}$ are obtained from solving the linear problems $\mathbf{K}_0^1\mathbf{U}_{11}^{1} = \mathbf{P}$, $\mathbf{K}_0^{i-1}\mathbf{U}_{11}^{i-1} = \mathbf{P}$, and $\mathbf{K}_0^{i}\mathbf{U}_{11}^{i} = \mathbf{P}$, respectively, with $\mathbf{K}_0^1$ and $\mathbf{K}_0^{i-1}$ being the assembled global tangent stiffness matrices at the start of the 1st and the $(i\text{-}1)th$ incremental loading steps, respectively.

The equilibrium equation at the jth iteration of the ith loading increment is given by

$$\mathbf{K}_{j-1}^{i}\Delta\mathbf{U}_j^i = \Delta\lambda_j^i\mathbf{P} + \mathbf{P}_{res} \qquad j \geq 2 \tag{62}$$

where $\mathbf{K}_{j-1}^{i}$ is the assembled global tangent stiffness matrix at the end of the $(j-1)th$ iteration, $\Delta\mathbf{U}_j^i$ the increments of the global variables obtained at the jth iteration, $\mathbf{P}_{res}$ the residual or unbalanced loading vector at the end of last iteration, and $\Delta\lambda_j^i$ the incremental loading parameter calculated in accordance with the general displacement controlling procedure [70] as follows

$$\Delta\lambda_j^i = -\frac{\mathbf{U}_{11}^{i-1\mathrm{T}}\mathbf{U}_{2j}^{i}}{\mathbf{U}_{11}^{i-1\mathrm{T}}\mathbf{U}_{1j}^{i}} \tag{63}$$

For convenience, Eq.(62) can be rewritten as

$$\mathbf{K}^{i}_{j-1}\mathbf{U}_{1}{}^{i}_{j} = \mathbf{P} \tag{64a}$$

$$\mathbf{K}^{i}_{j-1}\mathbf{U}_{2}{}^{i}_{j} = \mathbf{P}_{res} \tag{64b}$$

and the increments of the global variables given by

$$\Delta\mathbf{U}^{i}_{j} = \Delta\lambda^{i}_{j}\mathbf{U}_{1}{}^{i}_{j} + \mathbf{U}_{2}{}^{i}_{j} \tag{65}$$

Considering that all the global variables are *additive* in the present incremental nonlinear solution procedure, the global variables $\mathbf{U}^{i}$ at the end of the ith load increment are updated by

$$\mathbf{U}^{i} = \mathbf{U}^{i-1} + \sum_{j=1}^{m}\Delta\mathbf{U}^{i}_{j} \tag{66}$$

where $\mathbf{U}^{i-1}$ is the state of the global variables at the end of the $(i-1)th$ load increment, and m the number of iterations at the ith load increment.

The iterative process is terminated when the following convergence criterion is satisfied

$$\left|\frac{\mathbf{U}_{2}{}^{i}_{j}{}^{\mathrm{T}}\mathbf{P}_{res}}{\Delta\mathbf{U}_{1}^{i^{T}}\Delta\lambda^{i}_{1}\mathbf{P}}\right| \le err \tag{67}$$

where err represents a small error tolerance. In the numerical examples below, we set $err = 10^{-6}$.

6. Numerical examples

To demonstrate the reliability and computational accuracy of the present 9-node co-rotational quadrilateral shell element, designated as the Quad9 element, a hyperbolic-paraboloid shell with smooth mid-surface and six folded and multi-shell problems, all involving large displacement and large rotation are analyzed. The results are compared to those from other researchers [60-63].

6.1. Hyperbolic-paraboloid shell subjected to concentrated moment

Consider a hyperbolic-paraboloidal shell (Figure 3) with the geometry described by the

equation $Z = \frac{Y^2 - X^2}{40}$, and with thickness $a = 0.2m$. Its projection in the X-Y plane is a square with the two corners A and B lying in the X-Z plane of symmetry. The side length of the projected square is $L = 20m$. The corners A and B are not sharp, but are snipped by a cut normal to the X-Z plane, making an edge with width *b*, so only quadrilateral elements are used in the discretization. The shell material Young's modulus is $E = 10^4 \, kN/m^2$, and Poisson's ratio $\mu = 0.0$. This hyperbolic-paraboloidal shell is supported at two corners A and B (Figure 3) in such a way that these points of support can undergo displacements in the directions normal to the shell mid-surface at those points, whose displacements are constrained in the direction tangent to the curved symmetric line ADB that is the intersection of the shell and the X-Z plane of symmetry, which halves the shell into two mirror-image parts. Two opposite distributed moments $M = f \cdot \rho \cdot b$ are applied at the supported corner edges A and B, with *f* being the load factor, $\rho = 5kN \cdot m/m$ the density of the distributed moment, and *b* the width of the supported edges. This example was proposed by Basar and Ding [60] for testing large-rotation shell theory and for assessing shell finite elements in flexure with warped meshes.

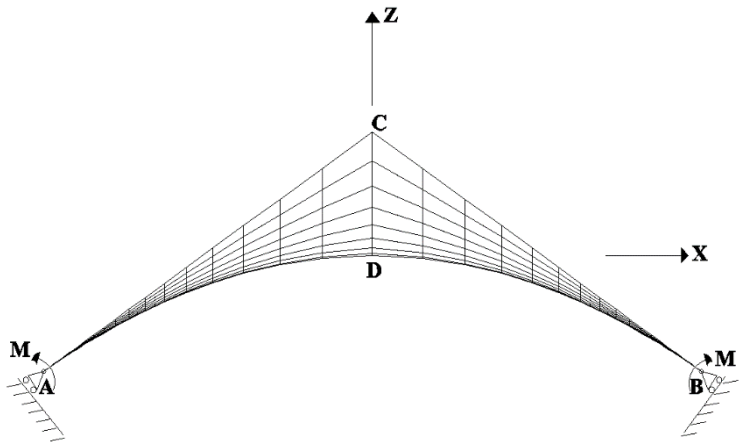

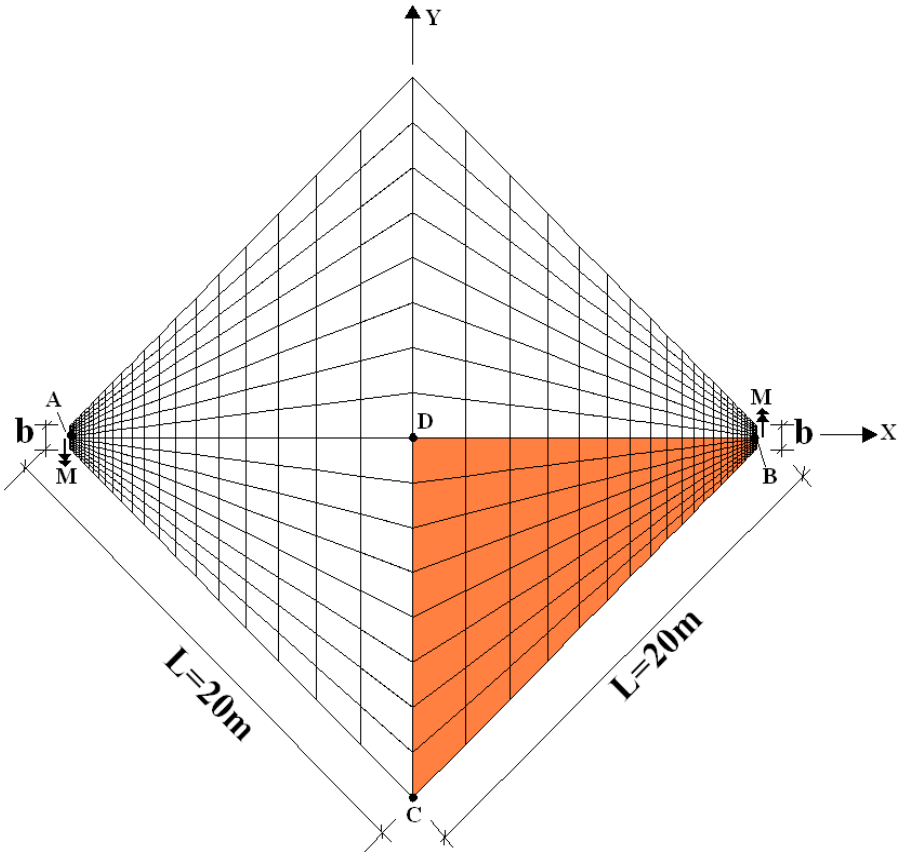

Figure 3. Hyperbolic paraboloidal shell loaded by two opposite moments along supported edges

Due to symmetry, only a quarter of the hyperbolic-paraboloidal shell (the colored zone in Figure 3) is modeled and analyzed using a mesh of 24×8 QUAD9 elements. The mesh is generated by reducing projected element lengths onto X-axis with a constant ratio of $q = 1/1.175$ in the direction of DA, while the projected element lengths onto Y-axis is divided equally. Figure 4 depicts the relationship between the applied load and the displacement of Point B relative to Point D. For comparison, the results from Chroscielewski et al. [61] using 8×3 CAMe16 elements (Lagrange family of 16-node displacement-rotation based shell elements), 12×4 SEMe9 elements (9-node stress resultant based semi-mixed shell element), 24×8 SEMe4 elements (4-node stress resultant based semi-mixed shell element), 12×4 ASCe9 elements (9-node assumed strain shell elements) and 24 × 8 ASCe4 elements (4-node assumed strain shell elements), respectively, are also represented in this figure. The solutions from using 24×8 QUAD9 elements agree well with those from using 8×3 CAMe16, 12×4 SEMe9, 12×4 ASCe9 and 24×8 ASCe4 elements, respectively.

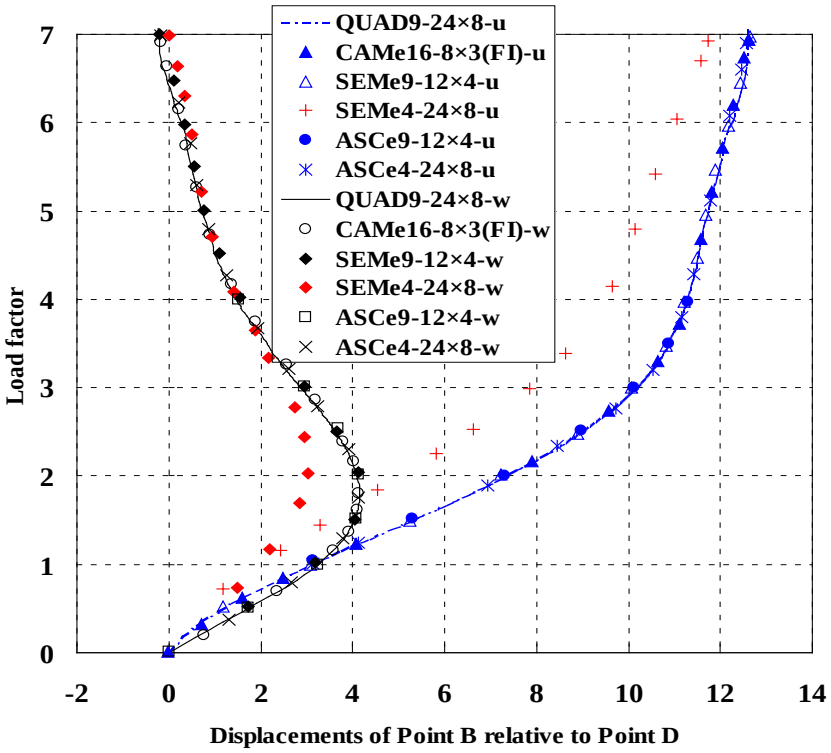

Figure 4. Applied load vs displacement of Point B relative to Point D

The deformed shapes of the hyperbolic-paraboloidal shell subjected to different magnitudes of applied moment (with load factor λ=0, 2, 3, 5, 7.23, respectively) calculated by using 28×4 QUAD9 elements are presented in Figure 5, where large displacements and large rotations can be clearly seen.

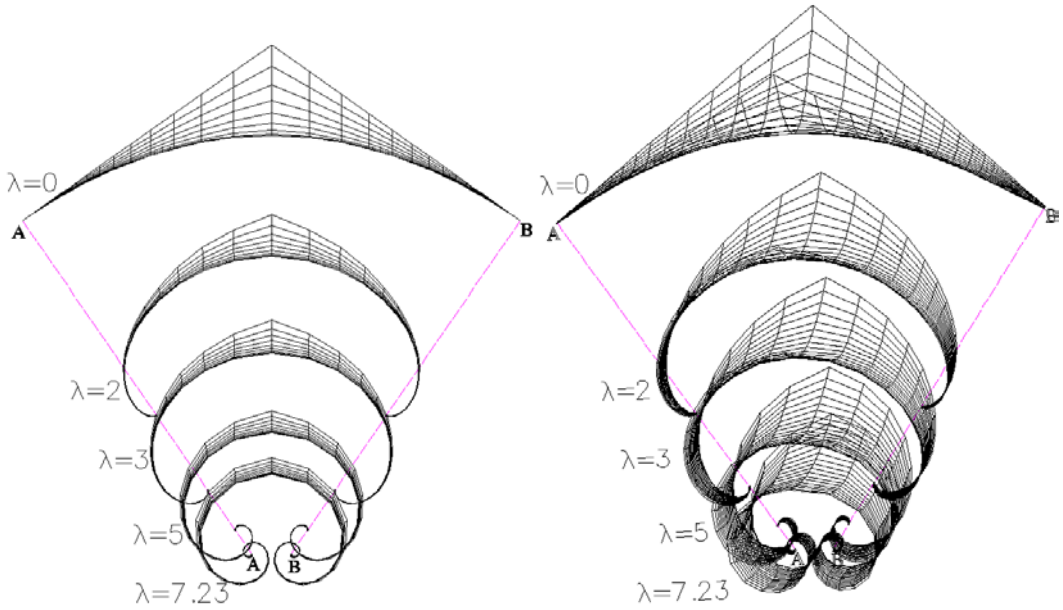

Figure 5. Deformed shapes of hyperbolic-paraboloidal shell subjected to different magnitudes of applied moments.

6.2. A right-angle cantilever subjected to distributed tip force/moment

Chroscielewski et al. [61] presented a right-angle cantilever plate clamped at one end, and loaded either by distributed force or distributed moment at the free end (Figures 6a,b). The plate has Young's modulus $E = 3 \times 10^7$, Poisson's ratio μ=0.0, with dimensions, length L=12, width b=3, and thickness a=0.03.

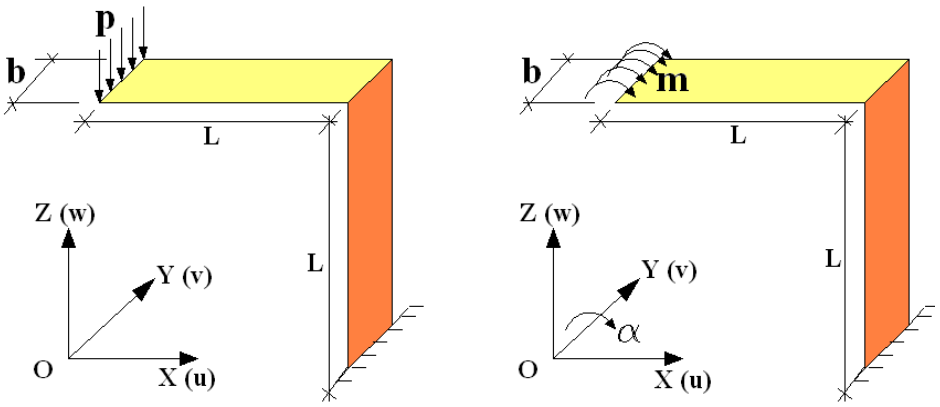

a) Distributed tip force b) Distributed tip moment

Figure 6. A right-angle cantilever subjected to distributed tip force/moment

Both cases of distributed tip force and tip moment are analyzed using the same mesh of (12+12) ×2 QUAD9 elements. The load-displacement curves for these two cases are depicted in Figure 7 and Figure 8, respectively. For comparison, the results obtained using the finite-element program ANSYS 18.0 [62] with a mesh of (12+12)×2 "Shell-81" elements (4-node quadrilateral shell element with six degree of freedoms per node, including a drilling rotation) are also depicted in these figures, showing a good agreement between the present QUAD9 element and the "shell-81" element of ANSYS [62].

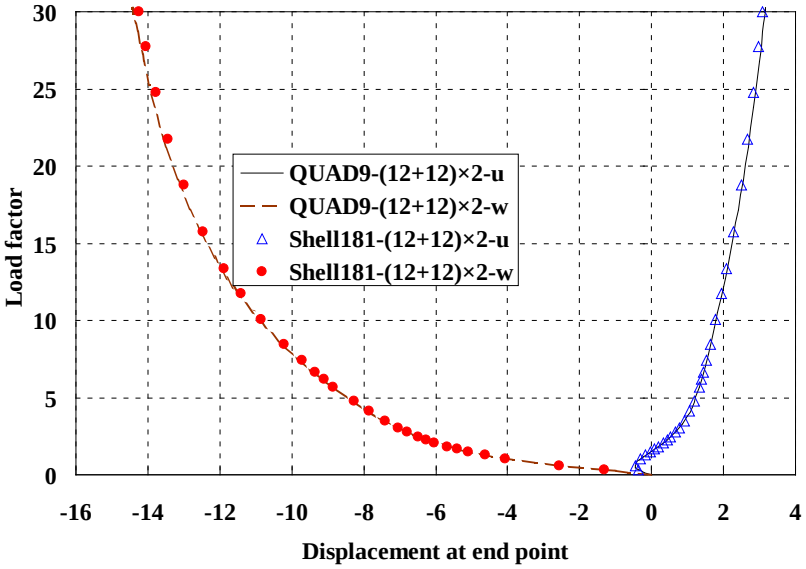

Figure 7. Load-displacement curve of right-angle cantilever subjected to distributed tip force

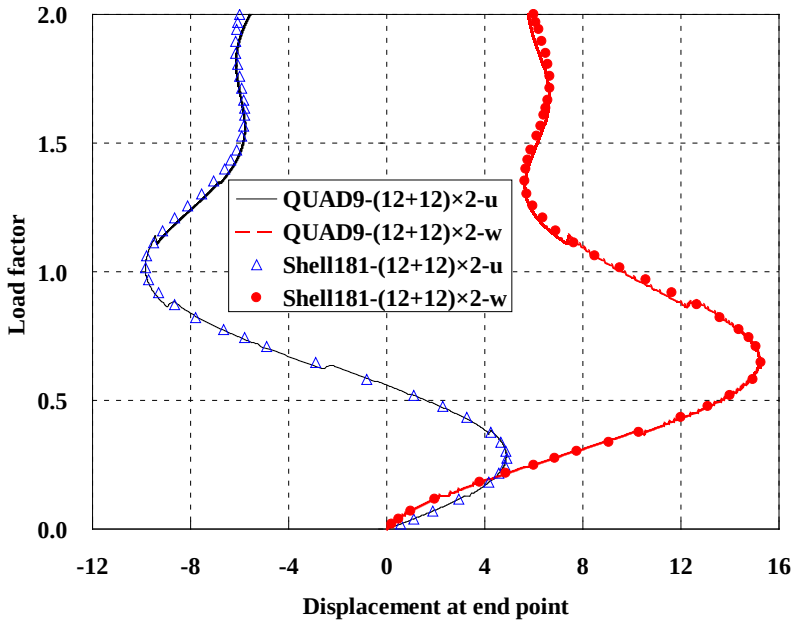

Figure 8. Load-displacement curve of right-angle cantilever subjected to distributed tip moment

The deformed shapes are presented in Figs. 9a,b, respectively, with clear large displacements and large rotations.

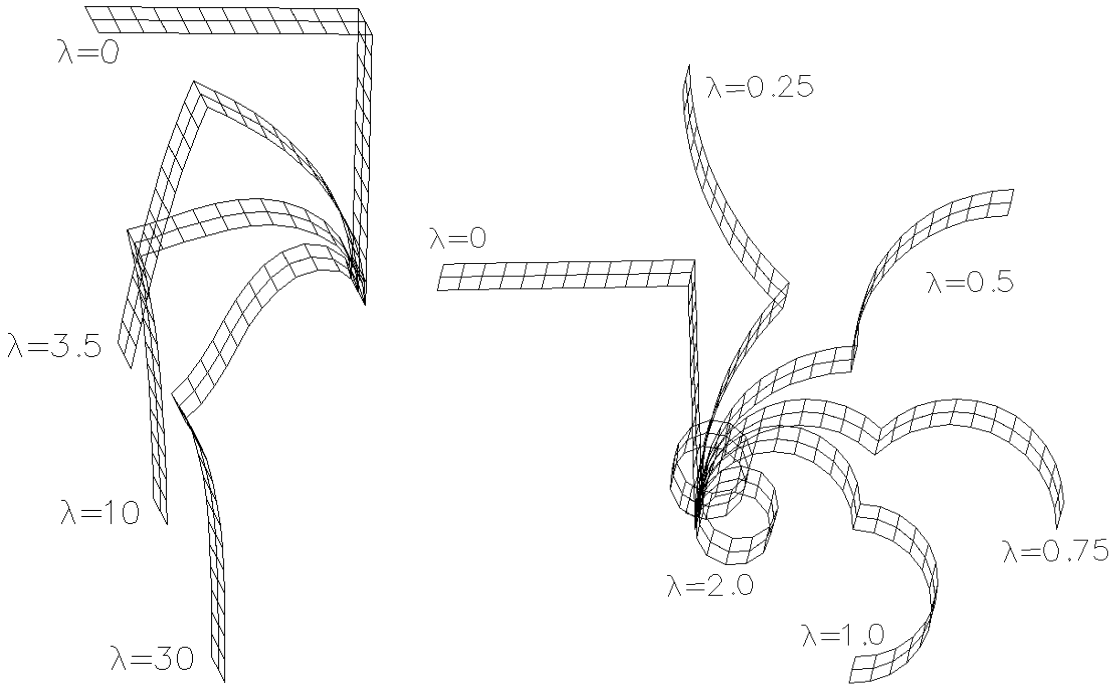

a) b)

Figure 9. Deformed shapes of right-angle cantilever under different magnitudes of distributed tip force and moment

6.3. Cantilever sickle shell subjected to lateral tip force

A cantilever sickle shell is subjected to a lateral force at the free end (Figure 10). The sickle shell has dimensions, radius R=5, length L=10, width B=1, and thickness a=0.01. The material parameters are Young's modulus $E = 3 \times 10^7$, and Poisson's ratio $\mu = 0.3$.

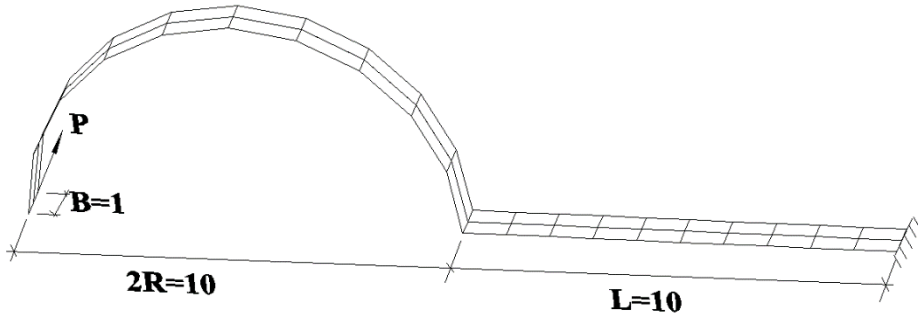

Figure 10. A cantilever sickle shell subjected to a lateral tip force

The sickle shell is discretized using (10+10)×2 QUAD9 elements, with the load-deflection curves at the midpoint of its free end given in Figure 11. The results from Chroscielewski et al. [61] using (10+10) × 2 SEMe9 elements and (10+10) × 2 SELe9 elements (9-node standard degenerated shell element with six degree of freedoms per node, including a drilling rotation) are

also presented in this figure. The results from using (10+10)×2 QUAD9 elements compare favourably with those from using (10+10)×2 SELe9 elements.

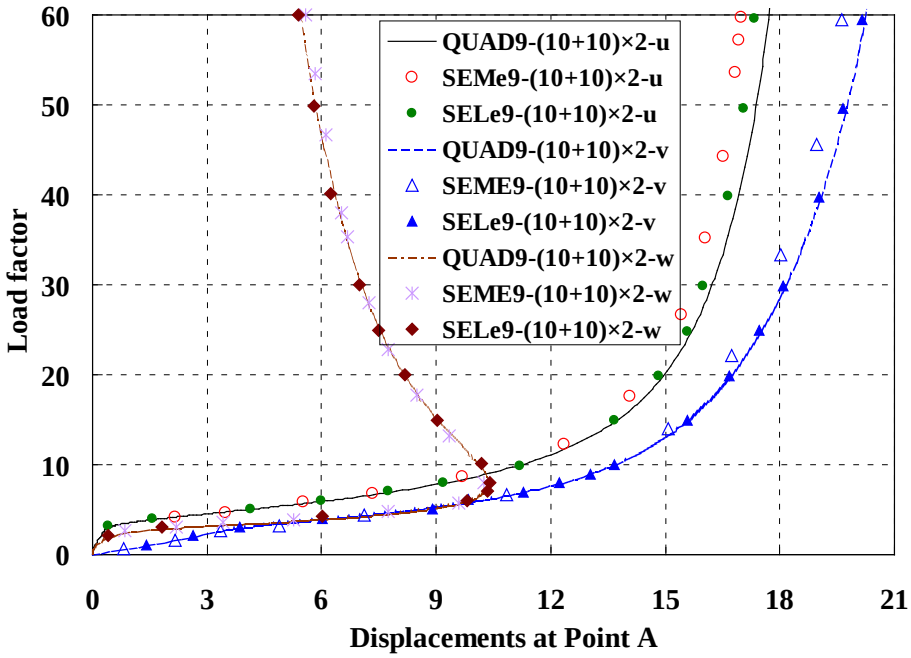

Figure 11. Load-displacement curves of cantilever sickle shell subjected to lateral tip force

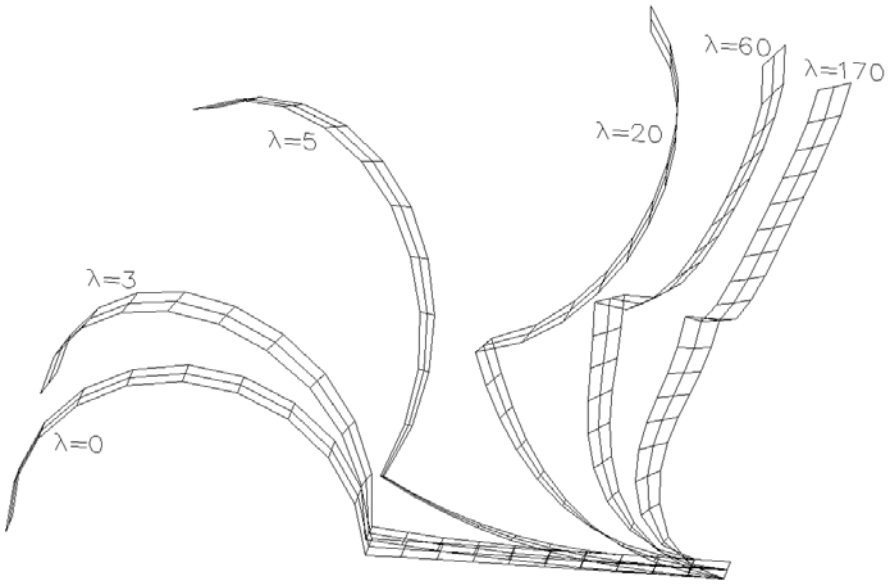

Figure 12. Deformed shape of cantilever sickle shell under different tip force magnitudes

The deformed shapes of the sickle shell at different magnitudes of the lateral tip force are presented in Figure 12.

6.4. Cantilever I-beam subjected to transversal tip force

Figure 13 depicts a cantilever I-beam subjected to a transverse tip force lying in the plane X-

Z, and located at the center of the free end. The beam geometry is characterized by length L=4800mm, flange width b=300mm, web height h_w=300mm, and thickness for both flange and web a=25mm. The beam's material properties are Young's modulus $E = 2 \times 10^5 \, N/mm^2$, and Poison's ratio $\mu = 0.3$.

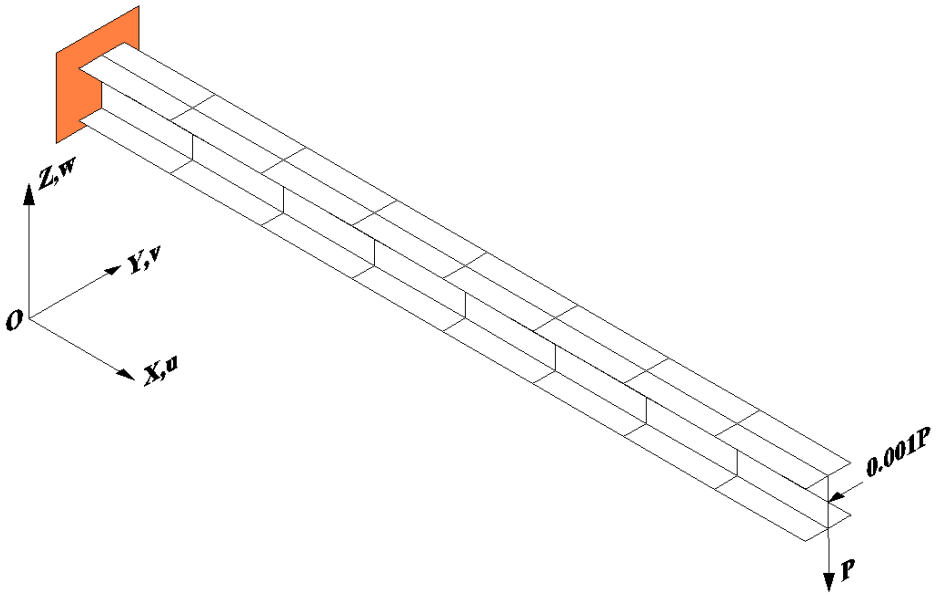

Figure 13. Cantilever I-beam subjected to transverse tip force

A mesh of (2+2+2)×8 QUAD9 elements is used to model this I-beam. To determine the critical load, a perturbation tip force, orthogonal to the applied force P and lying in the plane Y-Z, with magnitude P/1000, is applied at the centre of the free end before the beam approaches a critical state. Once instability occurs, i.e., when the beam begins to bend sideways, this perturbation load is subsequently removed. The load-displacement curves at the centre of the I-beam are presented in Figure 14. For comparison, the results from Chroscielewski et al. [61] using the meshes with (2+2+2) ×8 CAMe16 elements, (2+2+2)×8 CAMe9 elements (Lagrange family of 9-node displacement-rotation based shell elements with drilling rotations), (2+2+2)×8 SEMe4 elements and (2+2+2) ×8 SEMe9 elements, respectively are also presented in this figure. The solutions from using (2+2+2) ×8 QUAD9 elements fits very well with those from using (2+2+2)×8 CAMe16 elements.

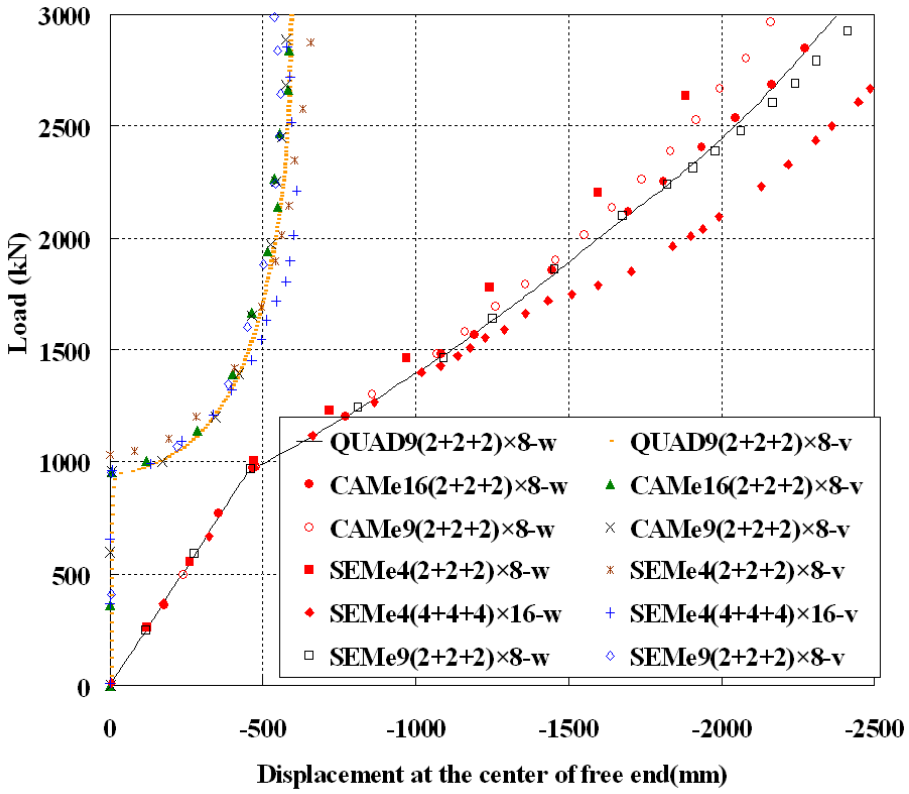

Figure 14. Load-displacement curves of cantilever I-beam subjected to a transverse tip force

The deformed shapes of the I-beam under the force magnitudes $\lambda = 1570$ and $\lambda = 2931$, with $P = \lambda P_{ref}$ and $P_{ref} = 1000N$, are presented in Figure 15, from which large displacement and large rotation can be observed.

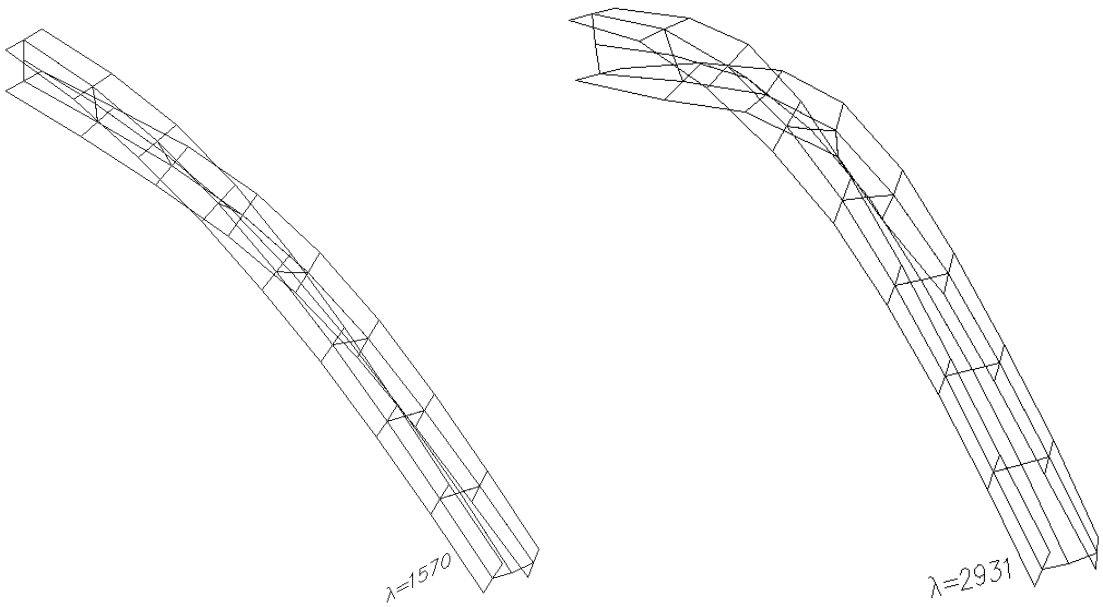

Figure 15. Deformed shapes of cantilever I-beam subjected to transverse tip force

6.5. Cantilever stiffened doubly-curved cylindrical panel

Shown in Figure 16 is a stiffened doubly-curved cylindrical panel fixed at one end, and subjected to a transverse force at the free end. The parameters for the shell geometry are length L=2, radius R=1, web height H=0.4, flange curvature angle $\alpha = 45^o$, and thickness a=0.01. The shell material properties are Young's modulus $E = 10^5$, and Poisson's $\mu = 0.25$.

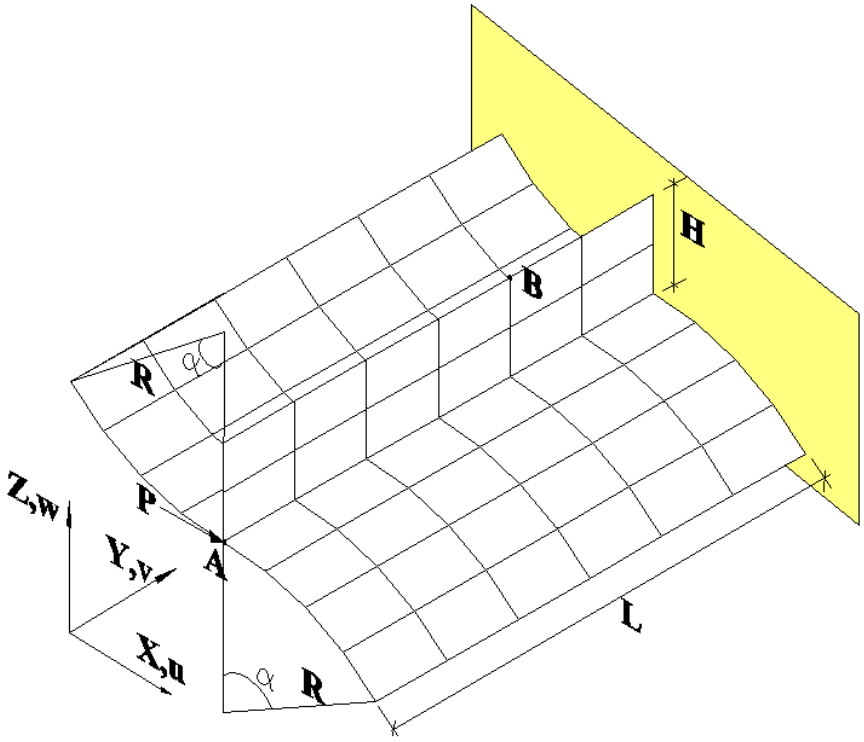

Figure 16. Cantilever stiffened doubly-curved cylindrical panel subjected to transverse tip force

The cantilever stiffened cylindrical panel is analyzed using a mesh of (4+4+2)×6 QUAD9 elements, with the resulting load-displacement curves at Points A and B presented in Figure 17. For comparison, the results from Chroscielewski et al. [61] using, respectively, (5+5+2)×6 CAMe16 elements, (4+4+2)×6 CAMe9 elements and (4+4+2)×6 SEMe9 elements, are also reported in this figure.

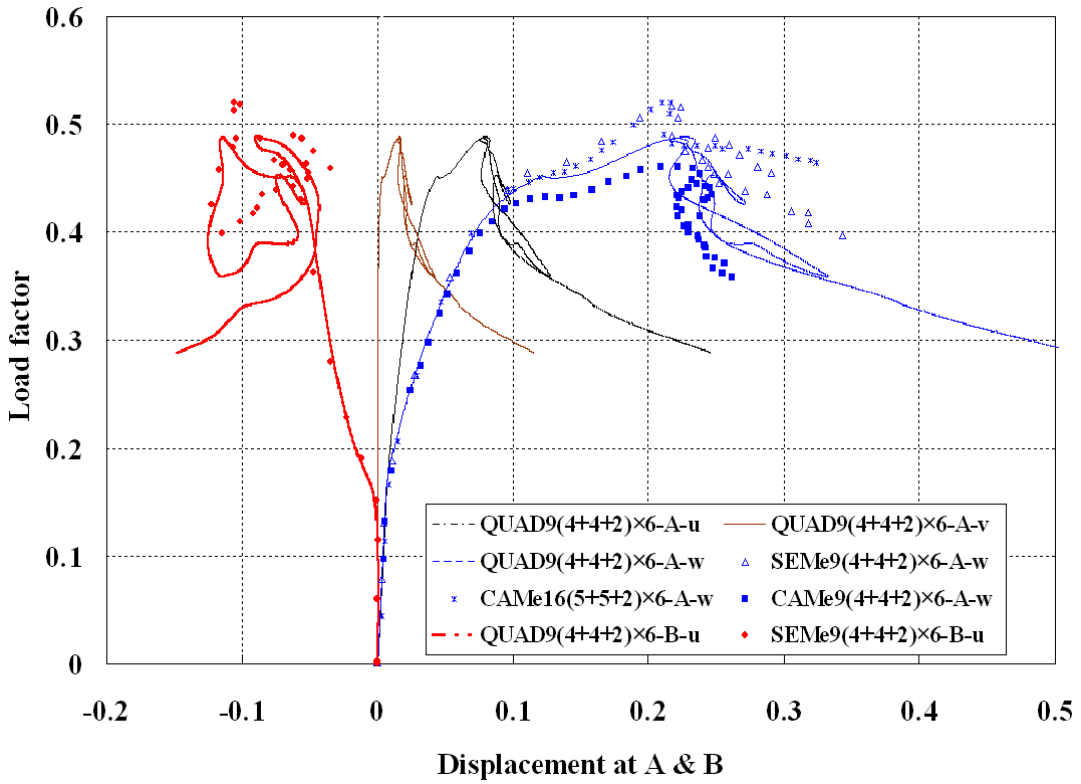

Figure 17. Load-displacement curves of cantilever stiffened cylindrical panel subjected to transverse tip force

The deformed shapes of the stiffened cylindrical panel at two different load levels are presented in Figure 18.

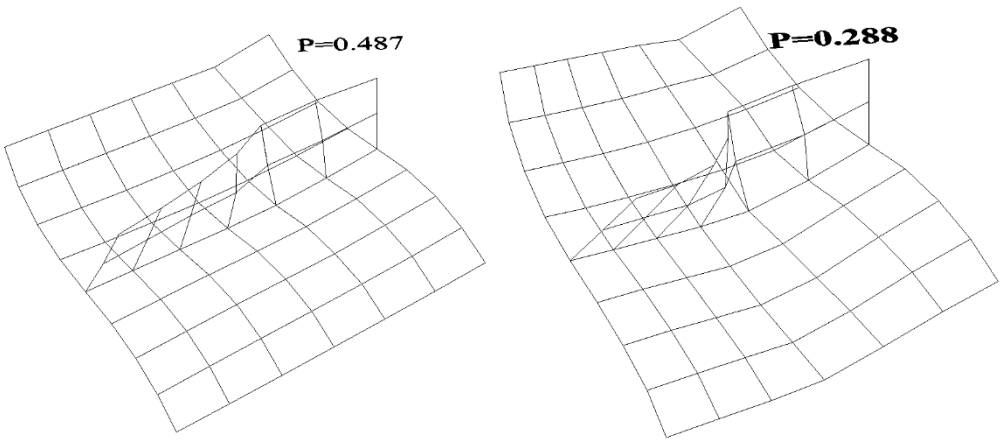

Figure 18. Deformed shapes of cantilever stiffened cylindrical panel at two different load magnitudes

6.6. Intersecting-plate structure

A structure consisting of three intersecting flat plates is subjected to six concentrated forces at

six different points, as shown Figure 19. The boundary conditions and reference loads are selected to bend the front plate and induce a torsional deflection of the middle plate. Consequently the induced torque must be supported by the clamped plate. The geometric dimensions of the intersecting plates are presented in Figure 19. The thickness of all three plates is $a = 0.02$. The material properties are Young's modulus $E = 2 \times 10^7$, and Poisson's $\mu = 0.25$. All loads are controlled by a load factor and the same reference load $P_{ref} = 2$ in the incremental nonlinear solution procedure.

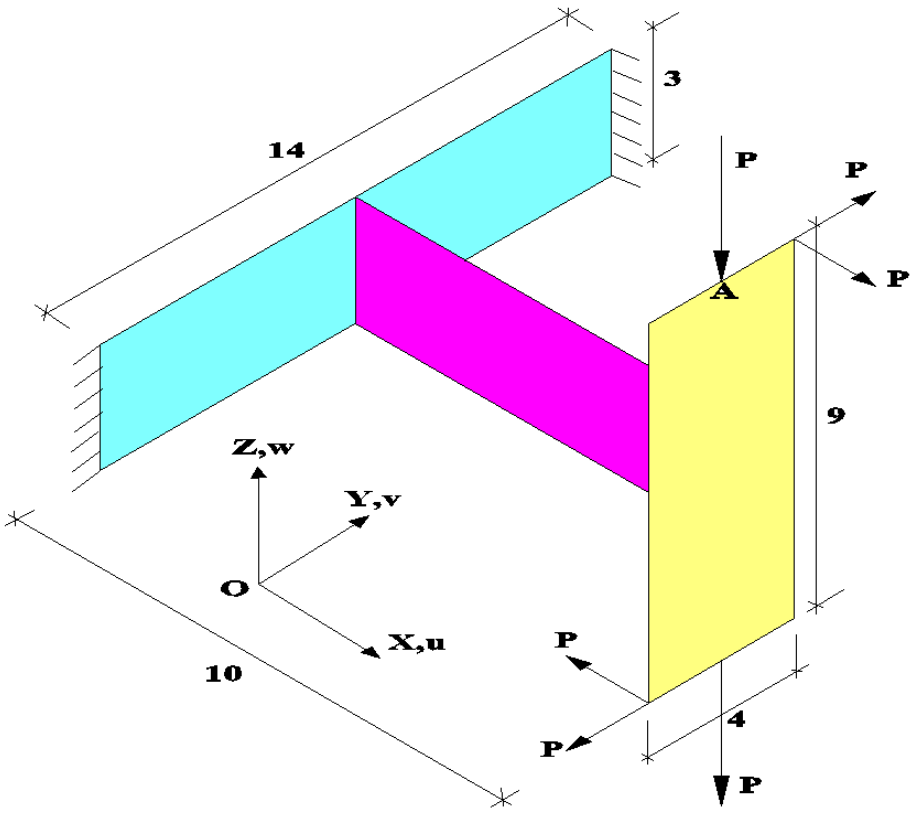

Figure 19. Intersecting plates subjected to six concentrated forces

A mesh with 3(8×24) QUAD9 elements is used to model the intersecting-plate structure, resulting in the load-displacement curves at Point A as depicted in Figure 20. The results obtained using, respectively, 3(8×24) CAMe16 elements [25], 3(12×36) and 3(36×72) EANS4 elements (a 4-node C_0 shell element with drilling degrees of freedom) [63] are also reported in this figure for comparison. The results from using 3(8×24) QUAD9 elements agree well with those from using 3(8×24) CAMe16 elements [25] and 3(36×72) EANS4 elements [63].

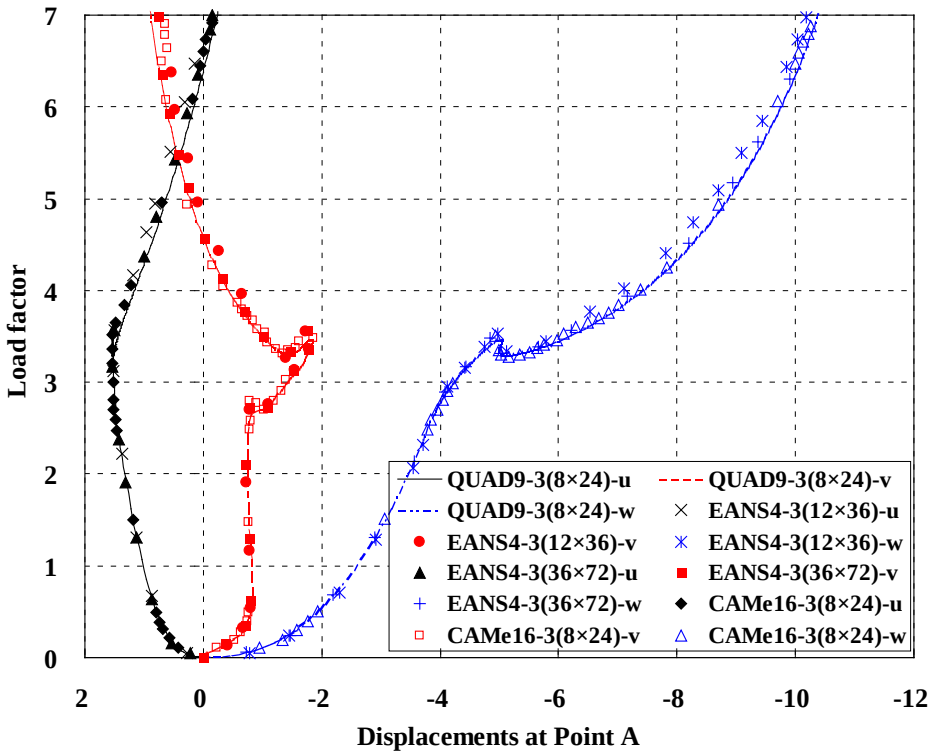

Figure 20. Load-displacement curves at Point A of intersecting-plate structure subjected to six concentrated forces

The initial shape and subsequent deformed shape of the intersecting-plate structure at the force magnitude $\lambda = 7.04$ are presented in Figure 21.

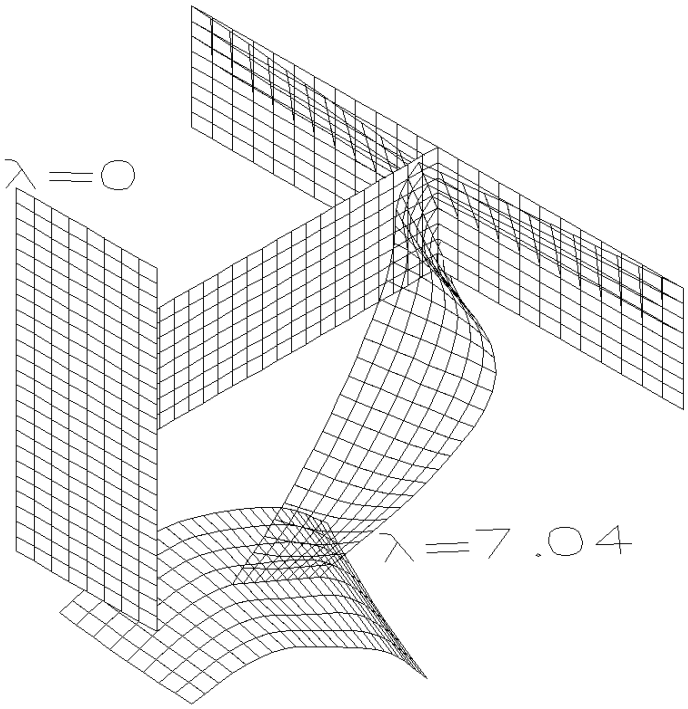

Figure 21. Initial and deformed shapes of intersecting-plate structure

7. Conclusions

A 9-node co-rotational curved quadrilateral shell element formulation is proposed in this paper for smooth, folded and multi-shell structures undergoing large displacements and large rotations. Different from other existing shell element formulations, *additive* and *communative* vectorial rotational variables are employed, resulting in symmetric element tangent stiffness matrices in both local and global coordinate systems. These vectorial rotational variables are components of normal vector or orientation vectors, which are (additive and commutative) polar / proper vectors, and not (non-additive and non-commutative) rotation axial / pseudo vectors. A sign-determination procedure for these vectorial rotational variables is introduced to update these variables in a nonlinear incremental solution procedure. To overcome membrane and shear locking phenomena, the membrane strains and the out-of-plane shear strains are replaced with assumed strains, using the Mixed Interpolation of Tensorial Components approach, for obtaining the element tangent stiffness matrices and the internal force vector. The reliability and computational accuracy of the present shell formulation are demonstrated in a number of smooth, folded and multi-shell problems involving large displacements and large rotations.

APPENDIX A: Various derivatives of strains with respect to local nodal variables

The first derivatives of membrane strains with respect to local nodal variables:

$$\mathbf{B}_m = \left\langle \mathbf{B}_{m1} \quad \mathbf{0} \quad \cdots \quad \mathbf{B}_{m9} \quad \mathbf{0} \right\rangle \tag{A-1a}$$

$$\mathbf{B}_{mi} = \begin{bmatrix} N_{i,x} & 0 & \dfrac{\partial(w+z)}{\partial x} N_{i,x} \\ 0 & N_{i,y} & \dfrac{\partial(w+z)}{\partial y} N_{i,y} \\ N_{i,y} & N_{i,x} & \dfrac{\partial(w+z)}{\partial y} N_{i,x} + \dfrac{\partial(w+z)}{\partial x} N_{i,y} \end{bmatrix} \qquad i=1,2,\ldots,9 \tag{A-1b}$$

where,

$$N_{i,x} = J_{11}^{-1} N_{i,\xi} + J_{12}^{-1} N_{i,\eta} \tag{A-2a}$$

$$N_{i,y} = J_{21}^{-1} N_{i,\xi} + J_{22}^{-1} N_{i,\eta} \tag{A-2b}$$

$J_{jk}^{-1}(j,k=1,2)$ is the component of inverse Jacobian matrix at *jth* row and *kth* column; $N_{i,\xi}$ and $N_{i,\eta}$ are respectively the first derivative of the shape function N_i with respect to ξ and η.

The first derivatives of shear strains with respect to local nodal variables:

$$\mathbf{B}_\gamma = \left\langle \mathbf{B}_{r1} \quad \mathbf{B}_{\gamma 2} \quad \cdots \quad \mathbf{B}_{r17} \quad \mathbf{B}_{r18} \right\rangle \tag{A-3a}$$

$$\mathbf{B}_{\gamma(2i-1)} = \begin{bmatrix} 0 & 0 & N_{i,x} \\ 0 & 0 & N_{i,y} \end{bmatrix} \qquad i=1,2,\ldots,9 \tag{A-3b}$$

$$\mathbf{B}_{\gamma(2i)} = \begin{bmatrix} N_i & 0 \\ 0 & N_i \end{bmatrix} \qquad i=1,2,\ldots,9 \tag{A-3c}$$

The first derivatives of bending strains with respect to local nodal variables:

$$\mathbf{B}_b = \left\langle \mathbf{0} \quad \mathbf{B}_{b1} \quad \cdots \quad \mathbf{0} \quad \mathbf{B}_{b9} \right\rangle \tag{A-4a}$$

$$\mathbf{B}_{bi} = \begin{bmatrix} N_{i,x} & 0 \\ 0 & N_{i,y} \\ N_{i,y} & N_{i,x} \end{bmatrix} \qquad i=1,2,\ldots,9 \tag{A-4b}$$

The second derivatives of membrane strains with respect to local nodal variables:

$$\left.\begin{aligned}
\left(\frac{\partial \mathbf{B}_m}{\partial \mathbf{u}_{\mathrm{L}}^{\mathrm{T}}}\right)_{1,5i-2,5j-2} &= N_{i,x}N_{j,x} \\
\left(\frac{\partial \mathbf{B}_m}{\partial \mathbf{u}_{\mathrm{L}}^{\mathrm{T}}}\right)_{2,5i-2,5j-2} &= N_{i,y}N_{j,y} \\
\left(\frac{\partial \mathbf{B}_m}{\partial \mathbf{u}_{\mathrm{L}}^{\mathrm{T}}}\right)_{3,5i-2,5j-2} &= N_{i,x}N_{j,y} + N_{i,y}N_{j,x}
\end{aligned}\right\} \quad i,j=1,2,\ldots,9. \tag{A-5}$$

where, three subscripts outside the parentheses in the right side of (A-5) represent the position of the component at the three dimensional matrix. The values of other unmentioned components of the three dimensional matrix are equal to zero.

APPENDIX B: Sub-matrices of transformation matrix T and its first derivatives with respect to global nodal variables

Sub-matrices of transformation matrix **T:**

$$\frac{\partial \mathbf{t}_k}{\partial \mathbf{d}_l^{\mathrm{T}}} = \frac{\partial \mathbf{R}}{\partial \mathbf{d}_l^{\mathrm{T}}}(\mathbf{d}_k + \mathbf{v}_{k0}) + \mathbf{R}\delta_{kl}\mathbf{I} = \left(\frac{\partial}{\partial \mathbf{d}_l^{\mathrm{T}}}\begin{bmatrix}\mathbf{e}_x^{\mathrm{T}} \\ \mathbf{e}_y^{\mathrm{T}} \\ \mathbf{e}_z^{\mathrm{T}}\end{bmatrix}\right)(\mathbf{d}_k + \mathbf{v}_{k0}) + \mathbf{R}\delta_{kl}\mathbf{I} \tag{B-1}$$

If Node *k* is away from intersections of non-smooth shell, two vectorial rotational variables are employed in global coordinate system, thus, the corresponding sub-matrices of $\mathbf{T}$ are evaluated as following,

$$\frac{\partial \boldsymbol{\theta}_k}{\partial \mathbf{d}_l^{\mathrm{T}}} = \frac{\partial \mathbf{R}_h}{\partial \mathbf{d}_l^{\mathrm{T}}}\mathbf{p}_k = \left(\frac{\partial}{\partial \mathbf{d}_l^{\mathrm{T}}}\begin{bmatrix}\mathbf{e}_x^{\mathrm{T}} \\ \mathbf{e}_y^{\mathrm{T}}\end{bmatrix}\right)\mathbf{p}_k \tag{B-2}$$

$$\frac{\partial \boldsymbol{\theta}_k}{\partial \mathbf{n}_{gl}^{\mathrm{T}}} = \mathbf{R}_h\delta_{kl}\frac{\partial \mathbf{p}_k}{\partial \mathbf{n}_{gl}^{\mathrm{T}}} = \begin{bmatrix}\mathbf{e}_x^{\mathrm{T}} \\ \mathbf{e}_y^{\mathrm{T}}\end{bmatrix}\delta_{kl}\frac{\partial \mathbf{p}_k}{\partial \mathbf{n}_{gl}^{\mathrm{T}}} \tag{B-3}$$

In Eqs.(B-1) and (B-2)

$$\frac{\partial \mathbf{e}_x}{\partial \mathbf{d}_l^{\mathrm{T}}} = \frac{\partial \mathbf{e}_x}{\partial \mathbf{c}_{13}^{\mathrm{T}}}\frac{\partial \mathbf{c}_{13}}{\partial \mathbf{d}_l^{\mathrm{T}}} + \frac{\partial \mathbf{e}_x}{\partial \mathbf{c}_{24}^{\mathrm{T}}}\frac{\partial \mathbf{c}_{24}}{\partial \mathbf{d}_l^{\mathrm{T}}} \tag{B-4}$$

$$\frac{\partial \mathbf{e}_y}{\partial \mathbf{d}_l^{\mathrm{T}}} = \frac{\partial \mathbf{e}_y}{\partial \mathbf{c}_{13}^{\mathrm{T}}}\frac{\partial \mathbf{c}_{13}}{\partial \mathbf{d}_l^{\mathrm{T}}} + \frac{\partial \mathbf{e}_y}{\partial \mathbf{c}_{24}^{\mathrm{T}}}\frac{\partial \mathbf{c}_{24}}{\partial \mathbf{d}_l^{\mathrm{T}}} \tag{B-5}$$

$$\frac{\partial \mathbf{e}_z}{\partial \mathbf{d}_l^{\mathrm{T}}} = \frac{\partial\left(\mathbf{e}_x \times \mathbf{e}_y\right)}{\partial \mathbf{d}_l^{\mathrm{T}}} \tag{B-6}$$

In Eqs.(B-1)~ (B-6), *k*, *l*=1,2,…,9.

$$\frac{\partial \mathbf{e}_x}{\partial \mathbf{c}_{13}^{\mathrm{T}}} = \frac{1}{|\mathbf{c}_{13} - \mathbf{c}_{24}|}\left(\mathbf{I} - \mathbf{e}_x \otimes \mathbf{e}_x\right) \tag{B-7}$$

$$\frac{\partial \mathbf{e}_x}{\partial \mathbf{c}_{24}^{\mathrm{T}}} = \frac{-1}{|\mathbf{c}_{13} - \mathbf{c}_{24}|}\left(\mathbf{I} - \mathbf{e}_x \otimes \mathbf{e}_x\right) \tag{B-8}$$

$$\frac{\partial \mathbf{e}_y}{\partial \mathbf{c}_{13}^{\mathrm{T}}} = \frac{1}{|\mathbf{c}_{13} + \mathbf{c}_{24}|}\left(\mathbf{I} - \mathbf{e}_y \otimes \mathbf{e}_y\right) \tag{B-9}$$

$$\frac{\partial \mathbf{e}_y}{\partial \mathbf{c}_{24}^{\mathrm{T}}} = \frac{1}{|\mathbf{c}_{13} + \mathbf{c}_{24}|}\left(\mathbf{I} - \mathbf{e}_y \otimes \mathbf{e}_y\right) \tag{B-10}$$

$$\frac{\partial \mathbf{c}_{13}}{\partial \mathbf{d}_j^{\mathrm{T}}} = \pm\frac{1}{|\mathbf{v}_{13}|}\left(\mathbf{I} - \mathbf{c}_{13} \otimes \mathbf{c}_{13}\right) \tag{B-11}$$

in (B-11), *j*=1 or 3, and if *j*=1, then, "$\pm$" takes the value of "–", else if j =3, it takes the value of "+". For other cases, the right side of (B-11) is a zero matrix.

$$\frac{\partial \mathbf{c}_{24}}{\partial \mathbf{d}_j^{\mathrm{T}}} = \pm\frac{1}{|\mathbf{v}_{24}|}\left(\mathbf{I} - \mathbf{c}_{24} \otimes \mathbf{c}_{24}\right) \tag{B-12}$$

in (B-12), *j*=2 or 4, and if *j*=2, then, "$\pm$" takes the value of "–", else if j =4, it takes the value of "+". For other cases, the right side of (B-12) is a zero matrix.

$$\frac{\partial \mathbf{p}_k}{\partial \mathbf{n}_{gk}^{\mathrm{T}}} = \begin{bmatrix} \dfrac{\partial p_{k,X}}{\partial p_{k,n}} & \dfrac{\partial p_{k,X}}{\partial p_{k,m}} \\ \dfrac{\partial p_{k,Y}}{\partial p_{k,n}} & \dfrac{\partial p_{k,Y}}{\partial p_{k,m}} \\ \dfrac{\partial p_{k,Z}}{\partial p_{k,n}} & \dfrac{\partial p_{k,Z}}{\partial p_{k,m}} \end{bmatrix} \tag{B-13}$$

in (B-13), $p_{k,X}$, $p_{k,Y}$ and $p_{k,Z}$ represent the three components of shell mid-surface normal vector $\mathbf{p}_k$ in the directions of global coordinate axes -X,-Y and –Z, respectively. $p_{k,n}$ and $p_{k,m}$ are the two vectorial rotational variables at Node *k*, they are the two smallest components of $p_{k,X}$, $p_{k,Y}$ and $p_{k,Z}$, and

$$\frac{\partial p_{k,n}}{\partial p_{k,n}} = \frac{\partial p_{k,m}}{\partial p_{k,m}} = 1 \tag{B-14a}$$

$$\frac{\partial p_{k,l}}{\partial p_{k,n}} = -\frac{p_{k,n}}{p_{k,l}} \tag{B-14b}$$

$$\frac{\partial p_{k,l}}{\partial p_{k,m}} = -\frac{p_{k,m}}{p_{k,l}} \tag{B-14c}$$

in (B-14a~c), $l \neq n \neq m$, $l,n,m \in \{X,Y,Z\}$, and they may take different values at different node of the same element. Other components not mentioned are equal to zero in Eq. (B-13).

If Node *k* locates at an intersection of non-smooth shell, three vectorial rotational variables are employed in global coordinate system, they are three smaller components of the triad vectors of orientation matrix at Node *k*, and

$$\frac{\partial \boldsymbol{\theta}_i}{\partial \mathbf{d}_j^{\mathrm{T}}} = \frac{\partial \mathbf{R}_h}{\partial \mathbf{d}_j^{\mathrm{T}}} \mathbf{R}_i^{\mathrm{T}} \mathbf{R}_{i0} \mathbf{p}_{i0} = \frac{\partial}{\partial \mathbf{d}_j^{\mathrm{T}}} \begin{bmatrix} \mathbf{e}_x^{\mathrm{T}} \\ \mathbf{e}_y^{\mathrm{T}} \end{bmatrix} \mathbf{R}_i^{\mathrm{T}} \mathbf{R}_{i0} \mathbf{p}_{i0} \tag{B-15}$$

$$\frac{\partial \boldsymbol{\theta}_i}{\partial \mathbf{n}_{gj}^{\mathrm{T}}} = \delta_{ij} \mathbf{R}_h \frac{\partial \mathbf{R}_i^{\mathrm{T}}}{\partial \mathbf{n}_{gj}^{\mathrm{T}}} \mathbf{R}_{i0} \mathbf{p}_{i0} = \delta_{ij} \mathbf{R}_h \frac{\partial}{\partial \mathbf{n}_{gj}^{\mathrm{T}}} \begin{bmatrix} \mathbf{e}_{ix} & \mathbf{e}_{iy} & \mathbf{e}_{iz} \end{bmatrix} \mathbf{R}_{i0} \mathbf{p}_{i0} \tag{B-16}$$

The first derivative on the right side of Eq. (B-15) is the same as Eqs.(B-4)-(B-12), and the first derivative on the right side of Eq. (B-16) is evaluated as following,

$$\frac{\partial \mathbf{e}_{ix}}{\partial \mathbf{n}_{gi}^{\mathrm{T}}} = \frac{\partial \mathbf{e}_{iy}}{\partial \mathbf{n}_{gi}^{\mathrm{T}}} \times \mathbf{e}_{iz} + \mathbf{e}_{iy} \times \frac{\partial \mathbf{e}_{iz}}{\partial \mathbf{n}_{gj}^{\mathrm{T}}} \tag{B-17}$$

$$\frac{\partial \mathbf{e}_{iy}}{\partial \mathbf{n}_{gi}^{\mathrm{T}}} = \begin{bmatrix} \dfrac{\partial \mathbf{e}_{iy}}{\partial e_{iy,n}} & \dfrac{\partial \mathbf{e}_{iy}}{\partial e_{iy,m}} & \mathbf{0} \end{bmatrix} \tag{B-18}$$

$$\frac{\partial \mathbf{e}_{iz}}{\partial \mathbf{n}_{gi}^{\mathrm{T}}} = \begin{bmatrix} \dfrac{\partial \mathbf{e}_{iz}}{\partial e_{iy,n}} & \dfrac{\partial \mathbf{e}_{iz}}{\partial e_{iy,m}} & \dfrac{\partial \mathbf{e}_{iz}}{\partial e_{iz,n}} \end{bmatrix} \tag{B-19}$$

The components in Eqs. (B-18) and (B-19) are calculated as following,

$$\frac{\partial e_{iy,n}}{\partial e_{iy,n}} = 1; \qquad \frac{\partial e_{iy,m}}{\partial e_{iy,m}} = 1; \qquad \frac{\partial e_{iy,l}}{\partial e_{iy,n}} = -\frac{e_{iy,n}}{e_{iy,l}} \tag{B-20a~c}$$

$$\frac{\partial e_{iy,l}}{\partial e_{iy,m}} = -\frac{e_{iy,m}}{e_{iy,l}}; \qquad \frac{\partial e_{iz,n}}{\partial e_{iz,n}} = 1 \tag{B-20d~e}$$

$$\frac{\partial e_{iz,l}}{\partial e_{iy,n}} = \frac{1}{1-e_{iy,n}^2} \left(-\frac{\partial e_{iy,l}}{\partial e_{iy,n}} e_{iy,n} e_{iz,n} - e_{iy,l} e_{iz,n} - s_1 s_3 e_{iy,m} \frac{\partial c_0}{\partial e_{iy,n}} + 2 e_{iz,l} e_{iy,n} \right) \tag{B-20f}$$

$$\frac{\partial e_{iz,l}}{\partial e_{iy,m}} = \frac{1}{1-e_{iy,n}^2} \left(-\frac{\partial e_{iy,l}}{\partial e_{iy,m}} e_{iy,n} e_{iz,n} - s_1 s_3 c_0 \right) \tag{B-20g}$$

$$\frac{\partial e_{iz,l}}{\partial e_{iz,n}} = \frac{1}{1-e_{iy,n}^2}\left(-e_{iy,l}e_{iy,n} - s_1 s_3 e_{iy,m}\frac{\partial c_0}{\partial e_{iz,n}}\right) \tag{B-20h}$$

$$\frac{\partial e_{iz,m}}{\partial e_{iy,n}} = -\frac{e_{iz,l}}{e_{iz,m}}\frac{\partial e_{iz,l}}{\partial e_{iy,n}}; \qquad \frac{\partial e_{iz,m}}{\partial e_{iy,m}} = -\frac{e_{iz,l}}{e_{iz,m}}\frac{\partial e_{iz,l}}{\partial e_{iy,m}} \tag{B-20i~j}$$

$$\frac{\partial e_{iz,m}}{\partial e_{iz,n}} = \frac{-e_{iz,n}}{e_{iz,m}} - \frac{e_{iz,l}}{e_{iz,m}}\frac{\partial e_{iz,l}}{\partial e_{iz,n}} \tag{B-20k}$$

in Eqs.(B-20f)~(B-20h),

$$c_0 = \sqrt{1-e_{iy,n}^2 - e_{iz,n}^2} \tag{B-21a}$$

$$\frac{\partial c_0}{\partial e_{iy,n}} = \frac{-e_{iy,n}}{c_0}; \qquad \frac{\partial c_0}{\partial e_{iz,n}} = \frac{-e_{iz,n}}{c_0} \tag{B-21b~c}$$

The first derivatives of transformation matrix T's sub-matrices with respect to global nodal variables:

$$\frac{\partial^2 \mathbf{t}_i}{\partial \mathbf{d}_j^{\mathrm{T}} \partial \mathbf{u}_{\mathrm{G}}^{\mathrm{T}}} = \left[\frac{\partial^2 \mathbf{t}_i}{\partial \mathbf{d}_j^{\mathrm{T}} \partial \mathbf{d}_1^{\mathrm{T}}} \quad \mathbf{0} \quad \cdots \quad \frac{\partial^2 \mathbf{t}_i}{\partial \mathbf{d}_j^{\mathrm{T}} \partial \mathbf{d}_9^{\mathrm{T}}} \quad \mathbf{0}\right] \tag{B-22}$$

$$\frac{\partial^2 \boldsymbol{\theta}_i}{\partial \mathbf{d}_j^{\mathrm{T}} \partial \mathbf{u}_{\mathrm{G}}^{\mathrm{T}}} = \left[\frac{\partial^2 \boldsymbol{\theta}_i}{\partial \mathbf{d}_j^{\mathrm{T}} \partial \mathbf{d}_1^{\mathrm{T}}} \quad \frac{\partial^2 \boldsymbol{\theta}_i}{\partial \mathbf{d}_j^{\mathrm{T}} \partial \mathbf{n}_{g1}^{\mathrm{T}}} \quad \cdots \quad \frac{\partial^2 \boldsymbol{\theta}_i}{\partial \mathbf{d}_j^{\mathrm{T}} \partial \mathbf{d}_9^{\mathrm{T}}} \quad \frac{\partial^2 \boldsymbol{\theta}_i}{\partial \mathbf{d}_j^{\mathrm{T}} \partial \mathbf{n}_{g9}^{\mathrm{T}}}\right] \tag{B-23}$$

$$\frac{\partial^2 \boldsymbol{\theta}_i}{\partial \mathbf{n}_{gj} \partial \mathbf{u}_G^{\mathrm{T}}} = \left[\frac{\partial^2 \boldsymbol{\theta}_i}{\partial \mathbf{n}_{gj} \partial \mathbf{d}_1^{\mathrm{T}}} \quad \frac{\partial^2 \boldsymbol{\theta}_i}{\partial \mathbf{n}_{gj} \partial \mathbf{n}_{g1}^{\mathrm{T}}} \quad \cdots \quad \frac{\partial^2 \boldsymbol{\theta}_i}{\partial \mathbf{n}_{gj} \partial \mathbf{d}_9^{\mathrm{T}}} \quad \frac{\partial^2 \boldsymbol{\theta}_i}{\partial \mathbf{n}_{gj} \partial \mathbf{n}_{g9}^{\mathrm{T}}}\right] \tag{B-24}$$

In (B-22)~(B-24) , *i*, j=1,2,…9, and the sub-matrices are presented as following,

$$\begin{aligned}\frac{\partial^2 \mathbf{t}_i}{\partial \mathbf{d}_j^{\mathrm{T}} \partial \mathbf{d}_k^{\mathrm{T}}} &= \frac{\partial^2 \mathbf{R}}{\partial \mathbf{d}_j^{\mathrm{T}} \partial \mathbf{d}_k^{\mathrm{T}}}\left(\mathbf{d}_i + \mathbf{v}_{i0}\right) + \frac{\partial \mathbf{R}}{\partial \mathbf{d}_j^{\mathrm{T}}}\delta_{ik}\mathbf{I} + \frac{\partial \mathbf{R}}{\partial \mathbf{d}_k^{\mathrm{T}}}\delta_{ij}\mathbf{I} \\ &= \begin{bmatrix} \dfrac{\partial^2 \mathbf{e}_x^{\mathrm{T}}}{\partial \mathbf{d}_j^{\mathrm{T}} \partial \mathbf{d}_k^{\mathrm{T}}} \\ \dfrac{\partial^2 \mathbf{e}_y^{\mathrm{T}}}{\partial \mathbf{d}_j^{\mathrm{T}} \partial \mathbf{d}_k^{\mathrm{T}}} \\ \dfrac{\partial^2 \mathbf{e}_z^{\mathrm{T}}}{\partial \mathbf{d}_j^{\mathrm{T}} \partial \mathbf{d}_k^{\mathrm{T}}} \end{bmatrix}\left(\mathbf{d}_i + \mathbf{v}_{i0}\right) + \begin{bmatrix} \dfrac{\partial \mathbf{e}_x^{\mathrm{T}}}{\partial \mathbf{d}_j^{\mathrm{T}}} \\ \dfrac{\partial \mathbf{e}_y^{\mathrm{T}}}{\partial \mathbf{d}_j^{\mathrm{T}}} \\ \dfrac{\partial \mathbf{e}_z^{\mathrm{T}}}{\partial \mathbf{d}_j^{\mathrm{T}}} \end{bmatrix}\delta_{ik}\mathbf{I} + \begin{bmatrix} \dfrac{\partial \mathbf{e}_x^{\mathrm{T}}}{\partial \mathbf{d}_k^{\mathrm{T}}} \\ \dfrac{\partial \mathbf{e}_y^{\mathrm{T}}}{\partial \mathbf{d}_k^{\mathrm{T}}} \\ \dfrac{\partial \mathbf{e}_z^{\mathrm{T}}}{\partial \mathbf{d}_k^{\mathrm{T}}} \end{bmatrix}\delta_{ij}\mathbf{I} \end{aligned} \tag{B-25}$$

If Node k is away from intersections of non-smooth shell or the mid-surface of shell is smooth,

$$\frac{\partial^2\boldsymbol{\theta}_i}{\partial\mathbf{d}_j^{\mathrm{T}}\partial\mathbf{d}_k^{\mathrm{T}}}=\frac{\partial^2\mathbf{R}_h}{\partial\mathbf{d}_j^{\mathrm{T}}\partial\mathbf{d}_k^{\mathrm{T}}}\mathbf{p}_i=\begin{bmatrix}\dfrac{\partial^2\mathbf{e}_x^{\mathrm{T}}}{\partial\mathbf{d}_j^{\mathrm{T}}\partial\mathbf{d}_k^{\mathrm{T}}}\\ \dfrac{\partial^2\mathbf{e}_y^{\mathrm{T}}}{\partial\mathbf{d}_j^{\mathrm{T}}\partial\mathbf{d}_k^{\mathrm{T}}}\end{bmatrix}\mathbf{p}_i \tag{B-26}$$

$$\frac{\partial^2\boldsymbol{\theta}_i}{\partial\mathbf{d}_j^{\mathrm{T}}\partial\mathbf{n}_{gk}^{\mathrm{T}}}=\frac{\partial^2\mathbf{R}_h}{\partial\mathbf{d}_j^{\mathrm{T}}}\delta_{ik}\frac{\partial\mathbf{p}_i}{\partial\mathbf{n}_{gk}^{\mathrm{T}}}=\begin{bmatrix}\dfrac{\partial\mathbf{e}_x^{\mathrm{T}}}{\partial\mathbf{d}_j^{\mathrm{T}}}\\ \dfrac{\partial\mathbf{e}_y^{\mathrm{T}}}{\partial\mathbf{d}_j^{\mathrm{T}}}\end{bmatrix}\delta_{ik}\frac{\partial\mathbf{p}_i}{\partial\mathbf{n}_{gk}^{\mathrm{T}}} \tag{B-27}$$

$$\frac{\partial^2\boldsymbol{\theta}_i}{\partial\mathbf{n}_{gj}^{\mathrm{T}}\partial\mathbf{n}_{gk}^{\mathrm{T}}}=\mathbf{R}_h\delta_{ij}\delta_{ik}\frac{\partial^2\mathbf{p}_i}{\partial\mathbf{n}_{gj}^{\mathrm{T}}\partial\mathbf{n}_{gk}^{\mathrm{T}}} \tag{B-28}$$

In (B-25)~(B-28), *i*, *j*, *k*=1,2,…,9, the first derivatives in Eqs.(B-25) and (B-27) are calculated as Eqs.(B-4)-(B-12), and Eqs. (B-13)-(B-14c).

$$\begin{aligned}\frac{\partial^2\mathbf{e}_x}{\partial\mathbf{d}_j^{\mathrm{T}}\partial\mathbf{d}_k^{\mathrm{T}}}=&\left(\frac{\partial^2\mathbf{e}_x}{\partial^2\mathbf{c}_{13}^{\mathrm{T}}}\frac{\partial\mathbf{c}_{13}}{\partial\mathbf{d}_k^{\mathrm{T}}}+\frac{\partial^2\mathbf{e}_x}{\partial\mathbf{c}_{13}^{\mathrm{T}}\partial\mathbf{c}_{24}^{\mathrm{T}}}\frac{\partial\mathbf{c}_{24}}{\partial\mathbf{d}_k^{\mathrm{T}}}\right)\frac{\partial\mathbf{c}_{13}}{\partial\mathbf{d}_j^{\mathrm{T}}}+\frac{\partial\mathbf{e}_x}{\partial\mathbf{c}_{13}^{\mathrm{T}}}\frac{\partial^2\mathbf{c}_{13}}{\partial\mathbf{d}_j^{\mathrm{T}}\partial\mathbf{d}_k^{\mathrm{T}}}\\&+\left(\frac{\partial^2\mathbf{e}_x}{\partial\mathbf{c}_{24}^{\mathrm{T}}\partial\mathbf{c}_{13}^{\mathrm{T}}}\frac{\partial\mathbf{c}_{13}}{\partial\mathbf{d}_k^{\mathrm{T}}}+\frac{\partial^2\mathbf{e}_x}{\partial^2\mathbf{c}_{24}^{\mathrm{T}}}\frac{\partial\mathbf{c}_{24}}{\partial\mathbf{d}_k^{\mathrm{T}}}\right)\frac{\partial\mathbf{c}_{24}}{\partial\mathbf{d}_j^{\mathrm{T}}}+\frac{\partial\mathbf{e}_x}{\partial\mathbf{c}_{24}^{\mathrm{T}}}\frac{\partial^2\mathbf{c}_{24}}{\partial\mathbf{d}_j^{\mathrm{T}}\partial\mathbf{d}_k^{\mathrm{T}}}\end{aligned} \tag{B-29}$$

$$\begin{aligned}\frac{\partial^2\mathbf{e}_y}{\partial\mathbf{d}_j^{\mathrm{T}}\partial\mathbf{d}_k^{\mathrm{T}}}=&\left(\frac{\partial^2\mathbf{e}_y}{\partial^2\mathbf{c}_{13}^{\mathrm{T}}}\frac{\partial\mathbf{c}_{13}}{\partial\mathbf{d}_k^{\mathrm{T}}}+\frac{\partial^2\mathbf{e}_y}{\partial\mathbf{c}_{13}^{\mathrm{T}}\partial\mathbf{c}_{24}^{\mathrm{T}}}\frac{\partial\mathbf{c}_{24}}{\partial\mathbf{d}_k^{\mathrm{T}}}\right)\frac{\partial\mathbf{c}_{13}}{\partial\mathbf{d}_j^{\mathrm{T}}}+\frac{\partial\mathbf{e}_y}{\partial\mathbf{c}_{13}^{\mathrm{T}}}\frac{\partial^2\mathbf{c}_{13}}{\partial\mathbf{d}_j^{\mathrm{T}}\partial\mathbf{d}_k^{\mathrm{T}}}\\&+\left(\frac{\partial^2\mathbf{e}_y}{\partial\mathbf{c}_{24}^{\mathrm{T}}\partial\mathbf{c}_{13}^{\mathrm{T}}}\frac{\partial\mathbf{c}_{13}}{\partial\mathbf{d}_k^{\mathrm{T}}}+\frac{\partial^2\mathbf{e}_y}{\partial^2\mathbf{c}_{24}^{\mathrm{T}}}\frac{\partial\mathbf{c}_{24}}{\partial\mathbf{d}_k^{\mathrm{T}}}\right)\frac{\partial\mathbf{c}_{24}}{\partial\mathbf{d}_j^{\mathrm{T}}}+\frac{\partial\mathbf{e}_y}{\partial\mathbf{c}_{24}^{\mathrm{T}}}\frac{\partial^2\mathbf{c}_{24}}{\partial\mathbf{d}_j^{\mathrm{T}}\partial\mathbf{d}_k^{\mathrm{T}}}\end{aligned} \tag{B-30}$$

in Eqs.(B-29)~(B-30) , *j*, *k*=1,2,3,4.

$$\frac{\partial^2\mathbf{e}_x}{\partial^2\mathbf{c}_{13}^{\mathrm{T}}}=\frac{-1}{\left|\mathbf{c}_{13}-\mathbf{c}_{24}\right|}\left(\frac{\partial\mathbf{e}_x}{\partial\mathbf{c}_{13}^{\mathrm{T}}}\otimes\mathbf{e}_x+\mathbf{e}_x\otimes\frac{\partial\mathbf{e}_x}{\partial\mathbf{c}_{13}^{\mathrm{T}}}\right)-\frac{1}{\left|\mathbf{c}_{13}-\mathbf{c}_{24}\right|^2}\left(\mathbf{I}-\mathbf{e}_x\otimes\mathbf{e}_x\right)\otimes\mathbf{e}_x \tag{B-31}$$

$$\frac{\partial^2\mathbf{e}_x}{\partial\mathbf{c}_{13}^{\mathrm{T}}\partial\mathbf{c}_{24}^{\mathrm{T}}}=\frac{-1}{\left|\mathbf{c}_{13}-\mathbf{c}_{24}\right|}\left(\frac{\partial\mathbf{e}_x}{\partial\mathbf{c}_{24}^{\mathrm{T}}}\otimes\mathbf{e}_x+\mathbf{e}_x\otimes\frac{\partial\mathbf{e}_x}{\partial\mathbf{c}_{24}^{\mathrm{T}}}\right)+\frac{1}{\left|\mathbf{c}_{13}-\mathbf{c}_{24}\right|^2}\left(\mathbf{I}-\mathbf{e}_x\otimes\mathbf{e}_x\right)\otimes\mathbf{e}_x \tag{B-32}$$

$$\frac{\partial^2\mathbf{e}_x}{\partial^2\mathbf{c}_{24}^{\mathrm{T}}}=\frac{1}{\left|\mathbf{c}_{13}-\mathbf{c}_{24}\right|}\left(\frac{\partial\mathbf{e}_x}{\partial\mathbf{c}_{24}^{\mathrm{T}}}\otimes\mathbf{e}_x+\mathbf{e}_x\otimes\frac{\partial\mathbf{e}_x}{\partial\mathbf{c}_{24}^{\mathrm{T}}}\right)-\frac{1}{\left|\mathbf{c}_{13}-\mathbf{c}_{24}\right|^2}\left(\mathbf{I}-\mathbf{e}_x\otimes\mathbf{e}_x\right)\otimes\mathbf{e}_x \tag{B-33}$$

$$\frac{\partial^2\mathbf{e}_y}{\partial^2\mathbf{c}_{13}^{\mathrm{T}}}=\frac{1}{\left|\mathbf{c}_{13}+\mathbf{c}_{24}\right|}\left(-\frac{\partial\mathbf{e}_y}{\partial\mathbf{c}_{13}^{\mathrm{T}}}\otimes\mathbf{e}_y-\mathbf{e}_y\otimes\frac{\partial\mathbf{e}_y}{\partial\mathbf{c}_{13}^{\mathrm{T}}}\right)-\frac{1}{\left|\mathbf{c}_{13}+\mathbf{c}_{24}\right|^2}\left(\mathbf{I}-\mathbf{e}_y\otimes\mathbf{e}_y\right)\otimes\mathbf{e}_y \tag{B-34}$$

$$\frac{\partial^2\mathbf{e}_y}{\partial\mathbf{c}_{13}^{\mathrm{T}}\partial\mathbf{c}_{24}^{\mathrm{T}}}=\frac{-1}{\left|\mathbf{c}_{13}+\mathbf{c}_{24}\right|}\left(\frac{\partial\mathbf{e}_y}{\partial\mathbf{c}_{24}^{\mathrm{T}}}\otimes\mathbf{e}_y+\mathbf{e}_y\otimes\frac{\partial\mathbf{e}_y}{\partial\mathbf{c}_{24}^{\mathrm{T}}}\right)-\frac{1}{\left|\mathbf{c}_{13}-\mathbf{c}_{24}\right|^2}\left(\mathbf{I}-\mathbf{e}_y\otimes\mathbf{e}_y\right)\otimes\mathbf{e}_y \tag{B-35}$$

$$\frac{\partial^2 \mathbf{e}_y}{\partial^2 \mathbf{c}_{24}^{\mathrm{T}}} = \frac{-1}{\left|\mathbf{c}_{13}+\mathbf{c}_{24}\right|}\left(\frac{\partial \mathbf{e}_y}{\partial \mathbf{c}_{24}^{\mathrm{T}}}\otimes \mathbf{e}_y + \mathbf{e}_y \otimes \frac{\partial \mathbf{e}_y}{\partial \mathbf{c}_{24}^{\mathrm{T}}}\right) - \frac{1}{\left|\mathbf{c}_{13}+\mathbf{c}_{24}\right|^2}\left(\mathbf{I}-\mathbf{e}_y\otimes\mathbf{e}_y\right)\otimes \mathbf{e}_y \tag{B-36}$$

$$\frac{\partial^2 \mathbf{c}_{13}}{\partial \mathbf{d}_j \partial \mathbf{d}_k^{\mathrm{T}}} = \pm\left[\frac{-1}{\left|\mathbf{v}_{13}\right|}\left(\frac{\partial \mathbf{c}_{13}}{\partial \mathbf{d}_k^{\mathrm{T}}}\otimes \mathbf{c}_{13} + \mathbf{c}_{13}\otimes\frac{\partial \mathbf{c}_{13}}{\partial \mathbf{d}_k^{\mathrm{T}}}\right) - \frac{\pm 1}{\left|\mathbf{v}_{13}\right|^2}\left(\mathbf{I}-\mathbf{c}_{13}\otimes\mathbf{c}_{13}\right)\otimes\mathbf{c}_{13}\right] \tag{B-37}$$

In (B-37), j,k=1 or 3, and if j=1, then, the first "$\pm$" takes the value of "–", else if j =3, it takes the value of "+"; if k=1, then, the second "$\pm$" takes the value of "–", else if k=3, it takes the value of "+"; For other cases, the right side of (B-37) is a zero matrix.

$$\frac{\partial^2 \mathbf{c}_{24}}{\partial \mathbf{d}_j \partial \mathbf{d}_k^{\mathrm{T}}} = \pm\left[\frac{-1}{\left|\mathbf{v}_{24}\right|}\left(\frac{\partial \mathbf{c}_{24}}{\partial \mathbf{d}_k^{\mathrm{T}}}\otimes \mathbf{c}_{24} + \mathbf{c}_{24}\otimes\frac{\partial \mathbf{c}_{24}}{\partial \mathbf{d}_k^{\mathrm{T}}}\right) - \frac{\pm 1}{\left|\mathbf{v}_{24}\right|^2}\left(\mathbf{I}-\mathbf{c}_{24}\otimes\mathbf{c}_{24}\right)\otimes\mathbf{c}_{24}\right] \tag{B-38}$$

In (B-38), j,k=2 or 4, and if j=2, then, the first "$\pm$" takes the value of "–", else if j =4, it takes the value of "+"; if k=2, then, the second "$\pm$" takes the value of "–", else if k=4, it takes the value of "+"; For other cases, the right side of (B-38) is a zero matrix.

$$\frac{\partial^2 \mathbf{e}_z}{\partial \mathbf{d}_j^{\mathrm{T}} \partial \mathbf{d}_k^{\mathrm{T}}} = \frac{\partial^2\left(\mathbf{e}_x \times \mathbf{e}_y\right)}{\partial \mathbf{d}_j^{\mathrm{T}} \partial \mathbf{d}_k^{\mathrm{T}}} \tag{B-39}$$

in (B-39), j, k=1,2,3,4.

$$\frac{\partial^2 \mathbf{p}_i}{\partial \mathbf{n}_{gi}^{\mathrm{T}} \partial \mathbf{n}_{gi}^{\mathrm{T}}} = \begin{bmatrix} \dfrac{\partial^2 \mathbf{p}_i}{\partial p_{n_i}^2} & \dfrac{\partial^2 \mathbf{p}_i}{\partial p_{n_i}\partial p_{m_i}} \\ \dfrac{\partial^2 \mathbf{p}_i}{\partial p_{m_i}\partial p_{n_i}} & \dfrac{\partial^2 \mathbf{p}_i}{\partial p_{m_i}^2} \end{bmatrix} \tag{B-40}$$

$$\frac{\partial^2 \mathbf{p}_i}{\partial p_{n_i}^2} = \begin{Bmatrix} \dfrac{\partial^2 p_{iX}}{\partial p_{n_i}^2} \\ \dfrac{\partial^2 p_{iY}}{\partial p_{n_i}^2} \\ \dfrac{\partial^2 p_{iZ}}{\partial p_{n_i}^2} \end{Bmatrix};\quad \frac{\partial^2 \mathbf{p}_i}{\partial p_{m_i}^2} = \begin{Bmatrix} \dfrac{\partial^2 p_{iX}}{\partial p_{m_i}^2} \\ \dfrac{\partial^2 p_{iY}}{\partial p_{m_i}^2} \\ \dfrac{\partial^2 p_{iZ}}{\partial p_{m_i}^2} \end{Bmatrix};\quad \frac{\partial^2 \mathbf{p}_i}{\partial p_{n_i}\partial p_{m_i}} = \begin{Bmatrix} \dfrac{\partial^2 p_{iX}}{\partial p_{n_i}\partial p_{m_i}} \\ \dfrac{\partial^2 p_{iY}}{\partial p_{n_i}\partial p_{m_i}} \\ \dfrac{\partial^2 p_{iZ}}{\partial p_{n_i}\partial p_{m_i}} \end{Bmatrix} \tag{B-41a~c}$$

$$\frac{\partial^2 p_{l_i}}{\partial p_{n_i}^2} = -\frac{1}{p_{l_i}} - \frac{p_{n_i}^2}{p_{l_i}^3};\quad \frac{\partial^2 p_{l_i}}{\partial p_{m_i}^2} = -\frac{1}{p_{l_i}} - \frac{p_{m_i}^2}{p_{l_i}^3};\quad \frac{\partial^2 p_{l_i}}{\partial p_{n_i}\partial p_{m_i}} = -\frac{p_{n_i}\,p_{m_i}}{p_{l_i}^3} \tag{B-42a~c}$$

in (B-40)~(B-42c), i=1,2,…9.

If Node k locates at an intersection of non-smooth shell,

$$\frac{\partial^2 \boldsymbol{\theta}_i}{\partial \mathbf{d}_j^{\mathrm{T}} \partial \mathbf{d}_k^{\mathrm{T}}} = \frac{\partial^2 \mathbf{R}_h}{\partial \mathbf{d}_j^{\mathrm{T}} \partial \mathbf{d}_k^{\mathrm{T}}} \mathbf{R}_i^{\mathrm{T}} \mathbf{R}_{i0} \mathbf{p}_{i0} = \begin{bmatrix} \dfrac{\partial^2 \mathbf{e}_x^{\mathrm{T}}}{\partial \mathbf{d}_j^{\mathrm{T}} \partial \mathbf{d}_k^{\mathrm{T}}} \\ \dfrac{\partial^2 \mathbf{e}_y^{\mathrm{T}}}{\partial \mathbf{d}_j^{\mathrm{T}} \partial \mathbf{d}_k^{\mathrm{T}}} \end{bmatrix} \mathbf{R}_i^{\mathrm{T}} \mathbf{R}_{i0} \mathbf{p}_{i0} \tag{B-43}$$

The second derivatives on the right hand side of Eq. (B-43) are the same as Eqs.(B-29)-(B-39).

$$\frac{\partial^2 \boldsymbol{\theta}_i}{\partial \mathbf{d}_j^{\mathrm{T}} \partial \mathbf{n}_{gk}^{\mathrm{T}}} = \frac{\partial \mathbf{R}_h}{\partial \mathbf{d}_j^{\mathrm{T}}} \delta_{ik} \frac{\partial \mathbf{R}_i^{\mathrm{T}}}{\partial \mathbf{n}_{gk}^{\mathrm{T}}} \mathbf{R}_{i0} \mathbf{p}_{i0} = \begin{bmatrix} \dfrac{\partial \mathbf{e}_x^{\mathrm{T}}}{\partial \mathbf{d}_j^{\mathrm{T}}} \\ \dfrac{\partial \mathbf{e}_y^{\mathrm{T}}}{\partial \mathbf{d}_j^{\mathrm{T}}} \end{bmatrix} \delta_{ik} \begin{bmatrix} \dfrac{\partial \mathbf{e}_{ix}}{\partial \mathbf{n}_{gk}^{\mathrm{T}}} & \dfrac{\partial \mathbf{e}_{iy}}{\partial \mathbf{n}_{gk}^{\mathrm{T}}} & \dfrac{\partial \mathbf{e}_{iz}}{\partial \mathbf{n}_{gk}^{\mathrm{T}}} \end{bmatrix} \mathbf{R}_{i0} \mathbf{p}_{i0} \tag{B-44}$$

$$\begin{aligned} \frac{\partial^2 \boldsymbol{\theta}_i}{\partial \mathbf{n}_{gj}^{\mathrm{T}} \partial \mathbf{n}_{gk}^{\mathrm{T}}} &= \mathbf{R}_h \delta_{ij} \delta_{ik} \frac{\partial^2 \mathbf{R}_i^{\mathrm{T}}}{\partial \mathbf{n}_{gj}^{\mathrm{T}} \partial \mathbf{n}_{gk}^{\mathrm{T}}} \mathbf{R}_{i0} \mathbf{p}_{i0} \\ &= \mathbf{R}_h \delta_{ij} \delta_{ik} \begin{bmatrix} \dfrac{\partial^2 \mathbf{e}_{ix}}{\partial \mathbf{n}_{gj}^{\mathrm{T}} \partial \mathbf{n}_{gk}^{\mathrm{T}}} & \dfrac{\partial^2 \mathbf{e}_{iy}}{\partial \mathbf{n}_{gj}^{\mathrm{T}} \partial \mathbf{n}_{gk}^{\mathrm{T}}} & \dfrac{\partial^2 \mathbf{e}_{iz}}{\partial \mathbf{n}_{gj}^{\mathrm{T}} \partial \mathbf{n}_{gk}^{\mathrm{T}}} \end{bmatrix} \mathbf{R}_{i0} \mathbf{p}_{i0} \end{aligned} \tag{B-45}$$

$$\frac{\partial^2 \mathbf{e}_{ix}}{\partial \mathbf{n}_{gj}^{\mathrm{T}} \partial \mathbf{n}_{gk}^{\mathrm{T}}} = \frac{\partial^2 \mathbf{e}_{iy}}{\partial \mathbf{n}_{gj}^{\mathrm{T}} \partial \mathbf{n}_{gk}^{\mathrm{T}}} \times \mathbf{e}_{iz} + \mathbf{e}_{iy} \times \frac{\partial^2 \mathbf{e}_{iz}}{\partial \mathbf{n}_{gj}^{\mathrm{T}} \partial \mathbf{n}_{gk}^{\mathrm{T}}} + \frac{\partial \mathbf{e}_{iy}}{\partial \mathbf{n}_{gj}^{\mathrm{T}}} \times \frac{\partial \mathbf{e}_{iz}}{\partial \mathbf{n}_{gk}^{\mathrm{T}}} + \frac{\partial \mathbf{e}_{iy}}{\partial \mathbf{n}_{gk}^{\mathrm{T}}} \times \frac{\partial \mathbf{e}_{iz}}{\partial \mathbf{n}_{gi}^{\mathrm{T}}} \tag{B-46}$$

The first derivatives in Eqs.(B-44) and (B-46) are calculated as Eqs.(B-4)-(B-12), and Eqs. (B-18)-(B-21c). The second derivatives in Eqs.(B-45) and (B-46) are calculated as following,

$$\frac{\partial^2 e_{iy,l}}{\partial^2 e_{iy,n}} = -\frac{e_{iy,n}^2}{e_{iy,l}^3} - \frac{1}{e_{iy,l}}; \quad \frac{\partial^2 e_{iy,l}}{\partial e_{iy,n} \partial e_{iy,m}} = -\frac{e_{iy,n} e_{iy,m}}{e_{iy,l}^3}; \quad \frac{\partial^2 e_{iy,l}}{\partial^2 e_{iy,m}} = -\frac{e_{iy,m}^2}{e_{iy,l}^3} - \frac{1}{e_{iy,l}} \tag{B-47a~c}$$

$$\frac{\partial^2 c_0}{\partial^2 e_{iy,n}} = -\frac{e_{iy,n}^2}{c_0^3} - \frac{1}{c_0}; \quad \frac{\partial^2 c_0}{\partial e_{iy,n} \partial e_{iz,n}} = -\frac{e_{iy,n} e_{iz,n}}{c_0^3}; \quad \frac{\partial^2 c_0}{\partial^2 e_{iz,n}} = -\frac{e_{iz,n}^2}{c_0^3} - \frac{1}{c_0} \tag{B-47d~f}$$

$$\begin{aligned} \frac{\partial^2 e_{iz,l}}{\partial e_{iy,n}^2} = \frac{1}{1-e_{iy,n}^2} \Bigg\{ &-\left[\frac{\partial^2 e_{iy,l}}{\partial e_{iy,n}^2} e_{iy,n} + 2 \frac{\partial e_{iy,l}}{\partial e_{iy,n}} \right] e_{iz,n} - s_1 s_3 e_{iy,m} \frac{\partial^2 c_0}{\partial e_{iy,n}^2} + 2 e_{iy,n} \frac{\partial e_{iz,l}}{\partial e_{iy,n}} + 2 e_{iz,l} \Bigg\} \\ &+ \frac{2 e_{iy,n}}{1-e_{iy,n}^2} \frac{\partial e_{iz,l}}{\partial e_{iy,n}} \end{aligned} \tag{B-47g}$$

$$\frac{\partial^2 e_{iz,l}}{\partial e_{iy,n} \partial e_{iy,m}} = \frac{-1}{1-e_{iy,n}^2} \left[\left(\frac{\partial^2 e_{iy,l}}{\partial e_{iy,n} \partial e_{iy,m}} e_{iy,n} + \frac{\partial e_{iy,l}}{\partial e_{iy,m}} \right) e_{iz,n} + s_1 s_3 \frac{\partial c_0}{\partial e_{iy,n}} - 2 e_{iy,n} \frac{\partial e_{iz,l}}{\partial e_{iy,m}} \right] \tag{B-47h}$$

$$\frac{\partial^2 e_{iz,l}}{\partial e_{iy,n} \partial e_{iz,n}} = \frac{-1}{1-e_{iy,n}^2} \left(e_{iy,n} \frac{\partial e_{iy,l}}{\partial e_{iy,n}} + e_{iy,l} + s_1 s_3 e_{iy,m} \frac{\partial^2 c_0}{\partial e_{iy,n} \partial e_{iz,n}} + 2 e_{iy,n} \frac{\partial e_{iz,l}}{\partial e_{iz,n}} \right) \tag{B-47i}$$

$$\frac{\partial^2 e_{iz,l}}{\partial e_{iy,m}^2} = -\frac{e_{iy,n} e_{iz,n}}{1-e_{iy,n}^2} \frac{\partial^2 e_{iy,l}}{\partial e_{iy,m}^2} \tag{B-47j}$$

$$\frac{\partial^2 e_{iz,l}}{\partial e_{iy,m}\partial e_{iz,n}}=\frac{1}{1-e_{iy,n}^2}\left(-\frac{\partial e_{iy,l}}{\partial e_{iy,m}}e_{iy,n}-s_1s_3\frac{\partial c_0}{\partial e_{iz,n}}\right) \tag{B-47k}$$

$$\frac{\partial^2 e_{iz,l}}{\partial e_{iz,n}^2}=\frac{-s_1s_3e_{iy,m}}{1-e_{iy,n}^2}\frac{\partial^2 c_0}{\partial e_{iz,n}^2} \tag{B-47l}$$

$$\frac{\partial^2 e_{iz,m}}{\partial e_{iy,n}^2}=-\left[\frac{1}{e_{iz,m}}\left(\frac{\partial e_{iz,l}}{\partial e_{iy,n}}\right)^2+\frac{e_{iz,l}}{e_{iz,m}}\frac{\partial^2 e_{iz,l}}{\partial e_{iy,n}^2}\right]-\frac{1}{e_{iz,m}}\left(\frac{\partial e_{iz,m}}{\partial e_{iy,n}}\right)^2 \tag{B-47m}$$

$$\frac{\partial^2 e_{iz,m}}{\partial e_{iy,n}\partial e_{iy,m}}=-\frac{1}{e_{iz,m}}\frac{\partial e_{iz,l}}{\partial e_{iy,n}}\frac{\partial e_{iz,l}}{\partial e_{iy,m}}-\frac{e_{iz,l}}{e_{iz,m}}\frac{\partial^2 e_{iz,l}}{\partial e_{iy,n}\partial e_{iy,m}}-\frac{1}{e_{iz,m}}\frac{\partial e_{iz,m}}{\partial e_{iy,n}}\frac{\partial e_{iz,m}}{\partial e_{iy,m}} \tag{B-47n}$$

$$\frac{\partial^2 e_{iz,m}}{\partial e_{iy,n}\partial e_{iz,n}}=-\frac{1}{e_{iz,m}}\frac{\partial e_{iz,l}}{\partial e_{iy,n}}\frac{\partial e_{iz,l}}{\partial e_{iz,n}}-\frac{e_{iz,l}}{e_{iz,m}}\frac{\partial^2 e_{iz,l}}{\partial e_{iy,n}\partial e_{iz,n}}-\frac{1}{e_{iz,m}}\frac{\partial e_{iz,m}}{\partial e_{iy,n}}\frac{\partial e_{iz,m}}{\partial e_{iz,n}} \tag{B-47o}$$

$$\frac{\partial^2 e_{iz,m}}{\partial e_{iy,m}^2}=-\frac{1}{e_{iz,m}}\left(\frac{\partial e_{iz,l}}{\partial e_{iy,m}}\right)^2-\frac{e_{iz,l}}{e_{iz,m}}\frac{\partial^2 e_{iz,l}}{\partial e_{iy,m}^2}-\frac{1}{e_{iz,m}}\left(\frac{\partial e_{iz,m}}{\partial e_{iy,m}}\right)^2 \tag{B-47p}$$

$$\frac{\partial^2 e_{iz,m}}{\partial e_{iy,m}\partial e_{iz,n}}=-\frac{1}{e_{iz,m}}\frac{\partial e_{iz,l}}{\partial e_{iy,m}}\frac{\partial e_{iz,l}}{\partial e_{iz,n}}-\frac{e_{iz,l}}{e_{iz,m}}\frac{\partial^2 e_{iz,l}}{\partial e_{iy,m}\partial e_{iz,n}}-\frac{1}{e_{iz,m}}\frac{\partial e_{iz,m}}{\partial e_{iy,m}}\frac{\partial e_{iz,m}}{\partial e_{iz,n}} \tag{B-47q}$$

$$\frac{\partial^2 e_{iz,m}}{\partial e_{iz,n}^2}=-\frac{1}{e_{iz,m}}-\frac{e_{iz,l}}{e_{iz,m}}\frac{\partial^2 e_{iz,l}}{\partial e_{iz,n}^2}-\frac{1}{e_{iz,m}}\left(\frac{\partial e_{iz,l}}{\partial e_{iz,n}}\right)^2-\frac{1}{e_{iz,m}}\left(\frac{\partial e_{iz,m}}{\partial e_{iz,n}}\right)^2 \tag{B-47r}$$

Acknowledgements

This work was supported by National Natural Science Foundation of China (No.11672266).

References

[1] Chroscielewski J, Konopinska V, Pietraszkiewicz W. On modelling and non-linear elasto-plastic analysis of thin shells with deformable junctions. *Zamm-Zeitschrift fur Angewandte Mathematik und Mechanik* 2011; **91**(6): 477-484.

[2] Pietraszkiewicz W, Konopinska V. On unique kinematics for the branching shells. *International Journal of Solids and Structures* 2011; **48**(14-15): 2238-2244.

[3] Konopinska V, Pietraszkiewicz W. Exact resultant equilibrium conditions in the non-linear theory of branching and self-intersecting shells. *International Journal of Solids and Structures* 2007; **44**(1): 352-369.

[4] Pietraszkiewicz W, Konopinska V. Junctions in shell structures: A review. *Thin-Walled Structures* 2015; **95**: 310-334.

[5] Akian JL. Asymptotic analysis of bending-dominated shell junctions. *Journal De Mathematiques Pures Et Appliquees* 2005; **84**(6): 667-716.

[6] Argyris J. An excursion into large rotations. *Computer Methods in Applied Mechanics and Engineering* 1982; **32**(1-3): 85-155.

[7] Simo JC, Vu-Quoc L. A 3-dimensional finite-strain rod model .2. Computational aspects. *Computer Methods in Applied Mechanics and Engineering* 1986; **58**(1): 79-116.

[8] Ibrahimbegovic A, Brank B, Courtois P. Stress resultant geometrically exact form of classical shell model and vector-like parameterization of constrained finite rotations. *International Journal for Numerical Methods in Engineering* 2001; **52**(11): 1235-1252.

[9] Ibrahimbegovic A, Frey F, Kozar I. Computational aspects of vector-like parametrization of 3-dimensional finite rotations. *International Journal for Numerical Methods in Engineering* 1995; **38**(21): 3653-3673.

[10] Ibrahimbegovic A. On the choice of finite rotation parameters. *Computer Methods in Applied Mechanics and Engineering* 1997; **149**(1-4): 49-71.

[11] Brank B, Ibrahimbegovic A. On the relation between different parametrizations of finite rotations for shells. *Engineering Computations* 2001; **18**(7-8): 950-973.

[12] Allman DJ. A compatible triangular element including vertex rotations for plane elasticity analysis. *Computers & Structures* 1984; **19**(1-2): 1-8.

[13] Bauchau OA; Trainelli L. The vectorial parameterization of rotation. *Nonlinear Dynamics* 2003; **32**(1): 71-92.

[14] Nouromid B, Rankin CC. Finite rotation analysis and consistent linearization using projectors. *Computer Methods in Applied Mechanics and Engineering* 1991; **93**(3): 353-384.

[15] Argyris JH, Balmer H, Doltsinis, JS; Dunne, PC; Haase, M; Kleiber, M; Malejannakis, GA; Mlejnek, HP; Muller, M; Scharpf, DW. Finite-element method - natural approach. *Computer Methods in Applied Mechanics and Engineering* 1979; **17-8**(1): 1-106.

[16] Simo JC. A finite strain beam formulation - the 3-dimensional dynamic problem. Part I. *Computer Methods in Applied Mechanics and Engineering* 1985; **49**(1): 55-70.

[17] Ibrahimbegovic A. Stress resultant geometrically nonlinear shell theory with drilling rotations .1. A consistent formulation. *Computer Methods in Applied Mechanics and Engineering* 1994; **118**(3-4): 265-284.

[18] Ibrahimbegovic A, Frey F. Stress resultant geometrically nonlinear shell theory with drilling rotations .2. Computational aspects. *Computer Methods in Applied Mechanics and Engineering* 1994; **118**(3-4): 285-308.

[19] Ibrahimbegovic A, Frey F. Stress resultant geometrically nonlinear shell theory with drilling rotations .3. Linearized kinematics. *International Journal for Numerical Methods in Engineering* 1994; **37**(21): 3659-3683.

[20] Chroscielewski J, Kreja I, Sabik A, Witkowski W. Modeling of composite shells in 6-parameter nonlinear theory with drilling degree of freedom. *Mechanics of Advanced Materials and Structures* 2011; **18**(6): 403-419.

[21] Fox DD, Simo JC. A drill rotation formulation for geometrically exact shells. *Computer Methods in Applied Mechanics and Engineering* 1992; **98**(3): 329-343.

[22] Witkowski W. 4-Node combined shell element with semi-EAS-ANS strain interpolations in 6-parameter shell theories with drilling degrees of freedom. *Computational Mechanics* 2009; **43**(2): 307-319.

[23] Ibrahimbegovic A, Wilson EL. A unified formulation for triangular and quadrilateral flat shell finite-elements with 6 nodal degrees of freedom. *Communications in Applied Numerical*

Methods 1991; **7**(1): 1-9.

[24] Kebari H, Cassell AC. Non-conforming modes stabilization of a 9-node stress-resultant degenerated shell element with drilling freedom. *Computers & Structures* 1991; **40**(3): 569-580.

[25] Ibrahimbegovic A, Taylor RL, Wilson EL. A robust quadrilateral membrane finite-element with drilling degrees of freedom. *International Journal for Numerical Methods in Engineering* 1990; **30**(3): 445-457.

[26] Ibrahimbegovic A, Frey F. Variational-principles and membrane finite-elements with drilling rotations for geometrically nonlinear elasticity. *International Journal for Numerical Methods in Engineering* 1995; **38**(11): 1885-1900.

[27] Simo JC, Fox DD, Rifai MS. On a stress resultant geometrically exact shell-model. Part II. The linear-theory - computational aspects. *Computer Methods in Applied Mechanics and Engineering* 1989; **73**(1): 53-92.

[28] Dornisch W, Klinkel S. Treatment of Reissner-Mindlin shells with kinks without the need for drilling rotation stabilization in an isogeometric framework. *Computer Methods in Applied Mechanics and Engineering* 2014; **276**: 35-66.

[29] Vu-Quoc L, Tan XG. Optimal solid shells for non-linear analyses of multilayer composites. I. Statics. *Computer Methods in Applied Mechanics and Engineering* 2003; **192(9-10)**: 975-1016.

[30] Hauptmann R, Schweizerhof K. A systematic development of 'solid-shell' element formulations for linear and non-linear analyses employing only displacement degrees of freedom. *International Journal for Numerical Methods in Engineering* 1998; **42**(1): 49-69.

[31] Sze KY, Chan WK, Pian THH. An eight-node hybrid-stress solid-shell element for geometric non-linear analysis of elastic shells. *International Journal for Numerical Methods in Engineering* 2002; **55**(7): 853-878.

[32] Sze KY, Zheng SJ. A stabilized hybrid-stress solid element for geometrically nonlinear homogeneous and laminated shell analyses. *Computer Methods in Applied Mechanics and Engineering* 2002; **191(17-18)**: 1945-1966.

[33] Sze KY, Yao LQ. A hybrid stress ANS solid-shell element and its generalization for smart structure modelling. Part I - solid-shell element formulation. *International Journal for Numerical Methods in Engineering* 2000; **48**(4): 545-564.

[34] Izzuddin BA. An enhanced co-rotational approach for large displacement analysis of plates. *International Journal for Numerical Methods in Engineering* 2005; **64**(10): 1350-1374.

[35] Li ZX, Izzuddin BA, Vu-Quoc L, Rong ZH, Zhou X. A 3-node co-rotational triangular elasto-plastic shell element using vectorial rotational variables. *Advanced Steel Construction* 2017; **13**(3): 206-240.

[36] Li ZX, Xiang Y, Izzuddin BA, Vu-Quoc L, Zhuo X, Zhang CJ. A 6-node co-rotational triangular elasto-plastic shell element. *Computational Mechanics* 2015； **55**(5): 837-859..

[37] Li ZX, Zhuo X, Vu-Quoc L, Izzuddin BA, Wei HY. A 4-node co-rotational quadrilateral elasto-plastic shell element using vectorial rotational variables. *International Journal for Numerical Methods in Engineering* 2013; **95**(3): 181-211.

[38] Li ZX , Liu YF, Izzuddin BA, Vu-Quoc L. A stabilized co-rotational curved quadrilateral composite shell element. *International Journal for Numerical Methods in Engineering* 2011; **86**(8): 975-999.

[39] Li ZX, Izzuddin BA, Vu-Quoc L. A 9-node co-rotational quadrilateral shell element. *Computational Mechanics* 2008; **42**(6): 873-884.

[40] Li ZX, Vu-Quoc L. An efficient co-rotational formulation for curved triangular shell element. *International Journal for Numerical Methods in Engineering* 2007; **72**(9):1029-1062.

[41] Bathe KJ, Lee PS, Hiller JF. Towards improving the MITC9 shell element. *Computers and Structures* 2003; **81**: 477-489.

[42] Yang HTY, Saigal S, Masud A, Kapania RK. Survey of recent shell finite elements. *International Journal for Numerical Methods in Engineering* 2000; **47**(1-3): 101-127.

[43] Crisfield MA. Nonlinear Finite Element Analysis of Solid and Structures, *Vol.1: Essentials*. Wiley: Chichester, 1991.

[44] Crisfield MA. *Nonlinear Finite Element Analysis of Solid and Structures, Vol.2: Advanced topics*. Wiley: Chichester, 1996.

[45] Felippa CA, Haugen B. A unified formulation of small-strain corotational finite elements: I. Theory. *Computer Methods in Applied Mechanics and Engineering* 2005; **194**: 21-24.

[46] Crisfield MA. A consistent corotational formulation for nonlinear, 3-dimensional, beam-elements. *Computer Methods in Applied Mechanics and Engineering* 1990; **81**(2): 131-150.

[47] Kim M, Im S. A plate model for multilayer graphene sheets and its finite element implementation via corotational formulation. *Computer Methods in Applied Mechanics and Engineering* 2017; **325**: 102-138.

[48] Izzuddin BA, Liang Y. A hierarchic optimisation approach towards locking-free shell finite elements. *Computers & Structures*, DOI: 10.1016/j.compstruc.2017.08.010 (in press).

[49] Simo JC. (Symmetric) Hessian for geometrically nonlinear models in solid mechanics. Intrinsic definition and geometric interpretation. *Computer Methods in Applied Mechanics and Engineering* 1992; **96**:189‑200.

[50] Teh LH, Clarke MJ. Symmetry of tangent stiffness matrices of 3D elastic frame. *Journal of Engineering Mechanics*(ASCE) 1999; **125**:248‑251.

[51] Ritto-Corrêa M, Camotim D. Work-conjugacy between rotation-dependent moments and finite rotations. *International Journal of Solids and Structures* 2003; **40:** 2851–2873.

[52] Izzuddin BA. Conceptual issues in geometrically nonlinear analysis of 3d framed structures, *Computer Methods in Applied Mechanics and Engineering* 2001; **191:** 1029-1053.

[53] Le TN, Battini JM, Hjiaj M. A consistent 3D corotational beam element for nonlinear dynamic analysis of flexible structures. *Computer Methods in Applied Mechanics and Engineering* 2014; **269**: 538-565.

[54] Alsafadie R, Hjiaj M, Battini JM. Corotational mixed finite element formulation for thin-walled beams with generic cross-section. *Computer Methods in Applied Mechanics and Engineering* 2010; **199**: 49-52.

[55] Battini JM. A modified corotational framework for triangular shell elements. *Computer Methods in Applied Mechanics and Engineering* 2007; **196**(13-16): 1905-1914.

[56] Battini JM, Pacoste C. On the choice of the linear element for corotational triangular shells. *Computer Methods in Applied Mechanics and Engineering* 2006; **195**: 44-47.

[57] Goldstein H. *Classical Mechanics*. 2nd ed. Reading, MA: Addison-Wesley; 1980. p165.

[58] Simo JC, Tarnow N. A new energy and momentum conserving algorithm for the non-linear dynamics of shells. *International Journal for Numerical Methods in Engineering* 1994; **37**(15): 2527-2549.

[59] Simo JC, Rifai MS, Fox DD. On a stress resultant geometrically exact shell-model .6. Conserving algorithms for nonlinear dynamics. *International Journal for Numerical Methods in Engineering* 1992; **34** (1): 117-164.

[60] Basar Y, Ding YH. Finite-rotation elements for the non-linear analysis of thin shell structures. *International Journal of Solids and Structures* 1990; **26**(1): 83-97.

[61] Chroscielewski J, Makowski J, Stumpf H. Finite element analysis of smooth, folded and multi-shell structures. *Computer Methods in Applied Mechanics and Engineering* 1997; **141**(1-2): 1-46.

[62] ANSYS, Inc. Theory Reference Release 18.0. December 2016.

[63] Witkowski W. 4-Node combined shell element with semi-EAS-ANS strain interpolations in 6-parameter shell theories with drilling degrees of freedom. *Computational Mechanics* 2009; **43**(2): 307-319.

[64] Izzuddin BA, Liang Y. Bisector and zero-macrospin co-rotational systems for shell elements. *International Journal for Numerical Methods in Engineering* 2016; **105** (4): 286-320.

[65] Hughes TJR, Liu WK. Non-linear finite-element analysis of shells .1. 3-dimensional shells. *Computer Methods in Applied Mechanics and Engineering* 1981; **26**(3): 331-362.

[66] Hughes TJR, Liu WK. Non-linear finite-element analysis of shells .2. Two-dimensional shells. *Computer Methods in Applied Mechanics and Engineering* 1981; **27**(2): 167-181.

[67] Hughes TJR. *The Finite Element Method: Linear Static and Dynamic Finite Element Analysis.* New Jersey: Prentice-Hall Inc, Englewood Cliffs; 1987. P385-387.

[68] Belytschko T, Liu WK, Moran B, Elkhodary KI. *Nonlinear Finite Elements for Continua and Structures*. 2nd ed. Chichester: John Wiley & Sons, Ltd; 2014. P568-569.

[69] Li ZX, Vu-Quoc L. A mixed co-rotational 3D beam element formulation for arbitrarily large rotations. *Advanced Steel Construction* 2010; **6**(2): 767-787.

[70] Yang YB, Shieh MS. Solution method for nonlinear problems with multiple critical points. *AIAA Journal* 1990; **28**(12): 2110-2116.

[71] Steinbrecher I, Humer A, Vu-Quoc L. On the numerical modeling of sliding beams: A comparison of different approaches. *Journal of Sound and Vibration* 2017; **408**: 270-290.

[72] *HOTINT, a flexible multibody system dynamics freeware code in C++*, www.hotint.org.